Theoretical models for intensities of $d \rightarrow f$ transitions in electron-energy-loss spectra of rare-earth and actinide metals

Hans R. Moser* and Göran Wendin
Institute of Theoretical Physics, Chalmers University of Technology, S-412 96 Göteborg, Sweden
(Received 25 March 1991)

We calculate cross sections for electron-impact excitation of core electrons for La and Th metal within the local-density approximation (LDA), in particular, for the $4d \rightarrow 4f$ and $3d \rightarrow 4f$ transitions in La and for the $5d \rightarrow 5f$ and $4d \rightarrow 5f$ transitions in Th. The purpose is to account for the intensity variation of experimental electron-energy-loss spectra (EELS) when the incident-electron energy is lowered from high energies down to threshold, and, in particular, the appearance of structure due to exchange scattering involving capture into localized f levels. We use the distorted-wave approximation (DWA) at low incident energies and calculate direct and exchange inelastic-scattering cross sections for LS-resolved core excitations (neglecting spin-orbit interaction). In addition we have also made use of the Born approximation over the whole energy range. In general, the LDA DWA cross sections account rather well for the relative intensities of groups of spectral features connected with localized $d \rightarrow f$ excitations in EELS for La and Th metal. In La, the $3d \rightarrow 4f$ and $4d \rightarrow 4f$ transitions show similar exchange to direct inelastic-scattering cross-section ratios as functions of incident electron energy on the scale of the excitation energy. The ratio is of the order of unity at threshold. Our calculated branching ratios for ^3L to ^1P and ^1F to ^1P in La are in reasonable agreement with experimental trends. We find a clear difference between $4f$ and $5f$ elements in what concerns low-energy and threshold behavior. In particular, the $4d \rightarrow 5f$ transition in Th seems to be very special. Our calculated branching ratios show significant deviations from statistical weighting in the near-threshold region due to the effect of transition matrix elements. We conclude that LDA-based DWA calculations should provide a basis for deducing quantitative information about a variety of inelastic processes in rare-earth and actinide solids.

I. INTRODUCTION

Inelastic electron scattering allows rich possibilities for studying many-electron dynamics and correlation effects in solids.[1] For high incident-electron energies and small scattering angles only dipole transitions can be excited. In this limit, the electron-energy-loss spectrum (EELS) is equivalent to the photoabsorption spectrum. For low incident-electron energies, typically less than five times higher than the transition energy, exchange scattering may become important. The inelastically scattered electron may then participate in the dynamics of the target: the incident electron may be captured into a bound level while a core electron will be ejected. In particular, this allows strong spin-flip scattering through purely electrostatic interaction. Finally, for very low incident energies, in the region of the inelastic threshold, the incident electron may even be temporarily captured in a negative-ion two-electron–one-hole resonance.

Excitation spectra of lanthanide and actinide solids show prominent resonance effects due to the presence of localized or nearly localized empty $4f$ and $5f$ levels. $4d$-$4f$- and $5d$-$5f$-like transitions are particularly interesting since they present a wide spectrum of discrete and continuum resonance structures, and involve strongly collective transitions.[2,3] Recently, such spectra have been extensively studied using EELS in threshold regions,[4–14] revealing loss lines (Figs. 1–5 below) not observed in high-energy inelastic electron scattering[15] or in photoabsorption[16] or photoemission (including photoelectron yield and photodesorption).[17]

Capture processes into f levels have previously been experimentally studied in x-ray emission through appearance-potential spectroscopy,[18] bremsstrahlung isochromat spectroscopy (BIS),[19–23] and resonant BIS (Refs. 19–22) (for a theoretical approach to resonant BIS, see Refs. 3 and 24). Recently, such capture processes have become evident in EELS at incident-electron energies below a few times the threshold energy.[4–14] This includes some very recent studies on high-T_c superconductors.[12–14]

In this paper we present quantitative results for interpreting experimental EELS in rare-earth and actinide solids in inner-shell threshold regions. (A brief account of some of these results has been given in Ref. 25.) We have calculated low-energy, direct and exchange, angle-integrated inelastic-scattering cross sections for $3d \rightarrow 4f$ and $4d \rightarrow 4f$ excitations in La and $4d \rightarrow 5f$, $5d \rightarrow 5f$, and $4f \rightarrow 5f$ excitations in Th within the distorted-wave approximation (DWA). For comparison we have also calculated the direct inelastic cross sections using the Born approximation (BA). We have chosen La and Th as the simplest examples of lanthanide and actinide metals in order to avoid complications due to partially occupied f levels in the ground state (like in Ce or U). The calculation has been performed using an atomic model within the local-density approximation (LDA).[1,26,27] This should be adequate for describing the local aspects of the

core-excitation processes in $4f$ and $5f$ metals[28–30] and should provide a good description of *relative* intensities of loss structures with comparable loss energies at a given incident energy. On top of this, in order, for instance, to describe measured *absolute* variations of cross sections over wide energy ranges, one may have to include effects of the mean free path for the incident and scattered electrons.

In the case of $4d \rightarrow 4f$ excitation of La, the inelastic scattering processes may be written as

$$e^-(E) + \mathrm{La}(4d^{10}4f^0)\,{}^1S \rightarrow \mathrm{La}(4d^9 4f^1)\,{}^{2S+1}L_J + e^-(E')\ , \tag{1a}$$

$$e^-(E) \rightarrow e^-(E');\ 4d \rightarrow 4f \quad (\text{direct processes};\ J=1,3,5)\ , \tag{1b}$$

$$e^-(E) \rightarrow 4f;\ 4d \rightarrow e'(E') \quad (\text{exchange process})\ , \tag{1c}$$

where the angular momenta L and S take on all integer values in the range $1 \le L \le 5$ and $0 \le S \le 1$.

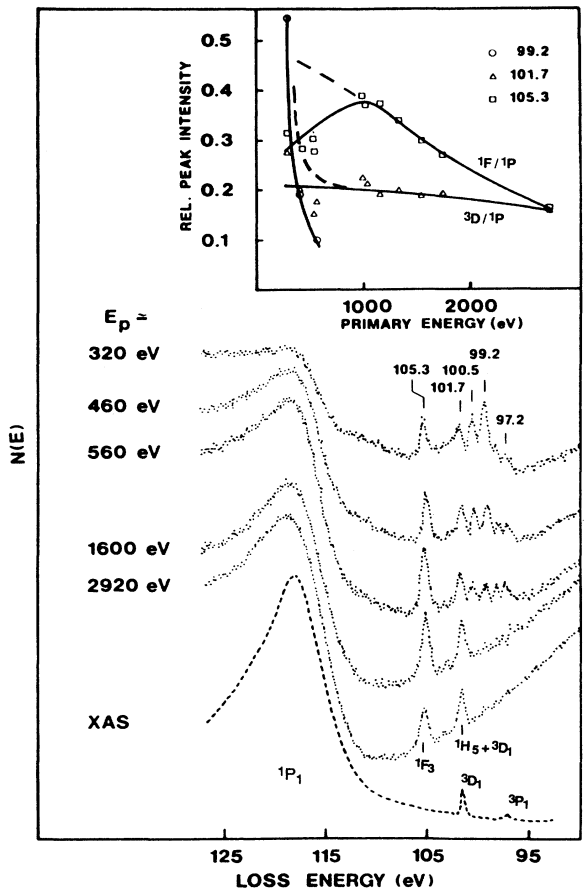

FIG. 1. Experimental low-energy EELS for La metal in the region of $4d \rightarrow 4f$ excitation, from Netzer, Strasser, and Matthew (Ref. 4). Comparison with x-ray absorption (XAS) (Rabe, Ref. 16). Dashed curves in the inset: *our alternative way of representing the data,* by subtracting a background under the ${}^1P_1$ giant dipole resonance before forming the ratio of peak heights.

In the absence of spin-orbit interaction, the direct process (1a) and (1b) *only* leads to total angular momentum transfer $J=1,3,5$ to $(4d^9 4f; 4\underline{d}4f)\,{}^1P_1, {}^1F_3, {}^1H_5$ final states,[31] corresponding to transferred orbital angular momenta $L=1,3,5$, respectively, and to transferred spin angular momentum $S=0$. The exchange process (1a) and (1c), on the other hand, admits *all* transferred angular momenta, $L=1,2,3,4,5$, and $S=0,1$, and therefore leads to all possible final states $(4d^9 4f; 4\underline{d}4f)\,{}^{1,3}L_J$ (in particular it interferes with the direct process to ${}^1P_1, {}^1F_3, {}^1H_5$ final states).

Experimental $4d \rightarrow 4f$ EELS for La metal are shown in Figs. 1 and 2 and for LaB_6 in Fig. 3. At low incident-electron energies E the spectra show a conglomerate of sharp, discrete $4\underline{d}4f\,{}^3L, {}^1L$ loss lines below the atomic $4d$ threshold followed by a sharp ${}^1F_3$ level (still below the atomic threshold), and finally above the atomic threshold a broad $4\underline{d}\varepsilon f\,{}^1P_1$ giant dipole resonance[2,3] ($4\underline{d}4f\,{}^1P_1$ in terms of LS structure of a single $4\underline{d}4f$ configuration[32]).

The general behavior of LS-dependent inelastic electron scattering cross sections is well understood from atomic theory and experiment. In this particular context, the problem was first discussed by Netzer, Strasser, and Matthew[4] and later by Moser and Wendin[25] and Clark *et al.*[14] Below we shall briefly illustrate three cases, $4\underline{d}4f$ excitation in La, $5\underline{d}5f$ in Th, and $3\underline{d}4f$ in La. The general picture for inelastic scattering with excitation (1a)–(1c) is then as follows.

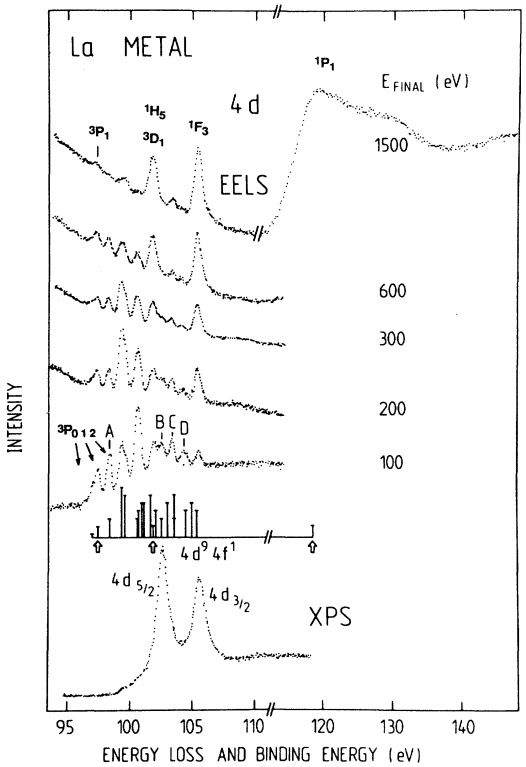

FIG. 2. Experimental low-energy EELS for La metal in the region of $4d \rightarrow 4f$ excitation, from Moser *et al.* (Ref. 6). The unlabeled fine structure in the 1500-eV EELS represents $J=3,5$ levels excited via the direct process through spin-orbit coupling to ${}^1F_3$ and ${}^1H_5$.

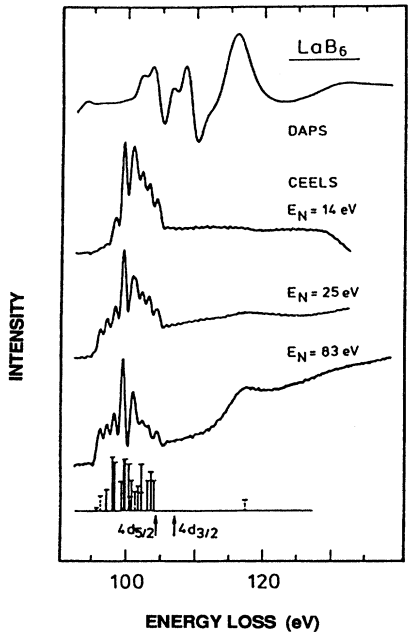

FIG. 3. Experimental very-low energy EELS for LaB_6 in the rgion of $4d \rightarrow 4f$ excitation, from Hinkers, Stiller, and Merz (Ref. 11).

(i) At high incident-electron energies E (i.e., much higher than the excitation energy in question) only the direct scattering process (1a) and (1b) is of interest. Moreover, only the *dipole*-allowed $J=1$ levels ($^3P_1, ^3D_1, ^1P_1$) will survive, and the EELS will tend towards the photoabsorption spectrum (curve labeled XAS in Fig. 1). The cross section is well described by the Born approximation (BA).

(ii) At intermediate energies E (e.g., $E_p = E = 2920$ and 1600 eV in Fig. 1; $E_{\text{final}} = E' = 1500$ eV in Fig. 2) the direct scattering process (1a) and (1b) is still the only one of interest. However, *nondipole* $J=3,5$ levels (spin-singlet $^1H_5$ and $^1F_3$ levels plus weaker spin-orbit driven spin-triplet levels) will grow relative to the $J=1$ levels.

(iii) At lower incident energies, for $E \approx 6-7$ times the threshold energy, the *exclusively exchange-driven* $J=2,4,6$ *levels* ($^3L_{2,4,6}$ plus $^1D_2$ and $^1G_4$) begin to gain intensity relative to the direct scattering $J=1,3,5$ levels, and rapidly become comparable in intensity to the direct scattering, spin-orbit driven $J=3,5$ levels (see the $E_{\text{final}} = E' = 600$ eV EELS in Fig. 2). This also means that *interference effects* between the direct and exchange amplitudes begin to be important.

(iv) At very low incident energies, for E tending towards the inelastic excitation threshold, the exchange scattering will dominate the EELS (except possibly for the continuum $^1P_1$ giant dipole resonance) and the entire $4\underline{d}4f\,^{2S+1}L_J$ structure in the 97–107-eV region will become very prominent, as seen in Fig. 3. The exchange-only process gives rise to a statistical distribution modified by LS-dependent matrix elements. This may be seen in Fig. 3 (see also Ref. 14), where the structure shows continuous development: at low but finite energy above threshold, there are still interference effects due to the direct process; very close to threshold, high-lying multiplet levels (here "$4\underline{d}4f$" ^1P) will be forbidden due to energy conservation.

A roughly statistical distribution of $(\underline{i}4f)\,^{1,3}L_J$ levels also appears in the context of relaxation of a core hole ($\underline{i}$) with localization of the screening charge.[33,34] This is illustrated by the $4d$ x-ray photoemission spectroscopy (XPS) spectrum in Fig. 2. Here a $4d$ core-hole potential pulls down an empty $4f$ level into the sea of conduction electrons. A conduction electron is scattered into this empty $4f$ level, forms a $4\underline{d}4f$ configuration, and gives rise to a nearly statistical $(4\underline{d}4f)\,^{1,3}L_J$ distribution (depends on the conduction electron density of states). Since the $4f$ level is very weakly hybridized with the conduction electrons, the filling process has a rather low probability. Therefore the satellite ("shake-down" and "shake-up") structure is quite weak, but clearly visible, in Fig. 2.

The case of $5\underline{d}5f$ excitation in Th metal is different in two important respects: (a) The $5d$ spin-orbit splitting is about 7 eV (3 eV for La $4d$), and (b) the $5f$ hybridization is quite strong. The larger spin-orbit splitting in the Th case leads to much larger weight on the $5\underline{d}5f\,^3D_1$ level;[2,3] this direct dipole excitation is therefore observable in the multiplet structure at low energies and leads to clear deviation from statistical weighting. The large $5f$ hybridization leads to a large probability for relaxation via filling of empty $5f$ levels,[35] as is evident in the XPS spectrum in Fig. 4 (cf. Fig. 2). Moreover, the $5f$ hybridization leads

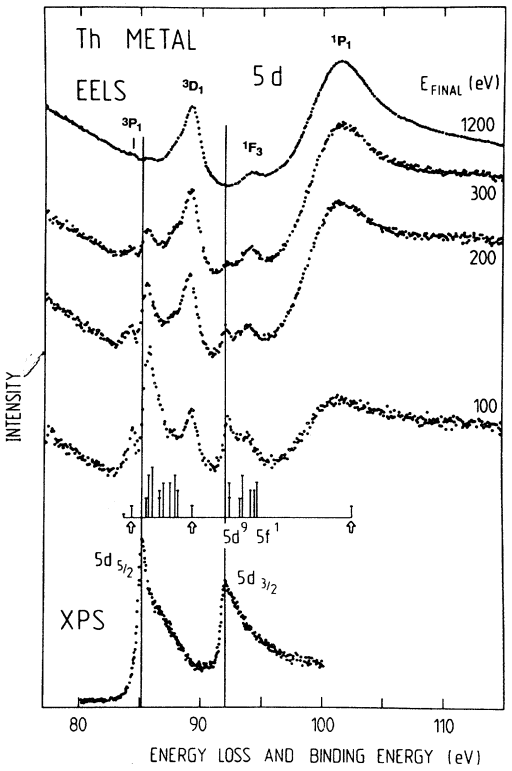

FIG. 4. Experimental low-energy EELS for Th metal in the region of $5d \rightarrow 5f$ excitation, from Moser *et al.* (Ref. 6).

to considerable broadening of the multiplet structure, making it largely impossible to resolve. (However, in most other respects the $5f$ levels may still be regarded as localized and atomiclike.)

Finally, the La $3d$-$4f$ spectra in Fig. 5 show still another picture. The $3d$-$4f$ exchange interaction is now relatively small (≈ 5 eV) while the spin-orbit splitting is large (17 eV). This leads to intermediate coupling with clear spin-orbit energy separation but with nonstatistical weighting. Since the $4f$ hybridization is weak, the $3d$ core-level XPS shows only weak shake-down satellite structure: relaxation by filling $4f$ levels has low probability.

The purpose of the present work is to provide a basis for interpretation of EELS such as discussed above, in particular for low incident energies (many of the above conclusions are based on the results of this investigation). The plan of the paper is as follows.

In Sec. II we describe the theoretical framework and present expressions for various types of excitation cross sections [LS-average, term-level (LS) resolved, spin polarization and spin-flip, etc.]. We also comment on aspects of many-electron dynamics. Section III presents numerical results for $d \rightarrow f$ excitation and ionization cross sections, while Sec. IV in particular deals with cross-section ratios with application to the relative intensities of peaks in the $(\underline{d}f)^{2S+1}L$ term-level structure.

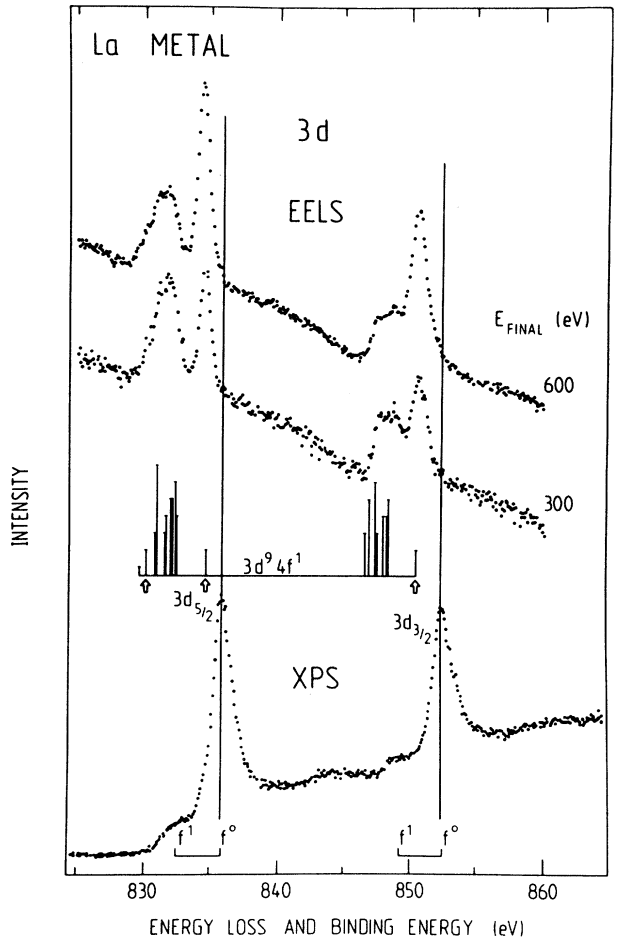

FIG. 5. Experimental low-energy EELS for La metal in the region of $3d \rightarrow 4f$ excitation, from Moser *et al.* (Ref. 6).

II. THEORETICAL MODELS OF THE SCATTERING PROCESSES

A. General

In a general theoretical treatment of inelastic scattering,[36–40] one must consider transitions between properly antisymmetrized states of the system of projectile plus target. As a consequence, the amplitude for transitions to physical final states will contain mixtures of direct and exchange scattering contributions. Some final states can only be reached via exchange scattering. On the other hand, there are no states which only can be reached by direct scattering.

In this work we calculate the incident- and scattered-electron wave functions in the potential of the target ground state,[41] and we describe the scattering process to first order in the electron-electron interaction, i.e., we use the distorted-wave Born approximation with exchange (DWA). The ion cores (targets) are described in the independent-electron approximation, and many-electron dynamics has to be accounted for explicitly through the appropriate response functions.

In an independent-electron approximation for the target, the amplitude for *direct* inelastic scattering with $\mathbf{k} \rightarrow \mathbf{k}'$ and $i \rightarrow n$ is given by

$$f_{\mathbf{k}'\mathbf{k}} = \langle \mathbf{k}' n | (1/r_{12}) | \mathbf{k} i \rangle \tag{2}$$

while the corresponding *exchange* amplitude with $\mathbf{k} \rightarrow n$ and $i \rightarrow \mathbf{k}'$ is given by

$$g_{\mathbf{k}'\mathbf{k}} = \langle n \mathbf{k}' | (1/r_{12}) | \mathbf{k} i \rangle \ . \tag{3}$$

The distorted waves $|\mathbf{k}\rangle$ and $|\mathbf{k}'\rangle$ for the incident and the inelastically scattered electrons are expanded in partial waves, in terms of radial one-electron wave functions $u_{kl}(r)$ calculated from the one-electron Schrödinger equation (energies in Rydberg units, $E = k^2$)

$$\left[\frac{d}{dr^2} + k^2 - V(r) - \frac{l(l+1)}{r^2} \right] u_{kl}(r) = 0 \tag{4}$$

with a one-electron potential $V(r)$ of the form (H stands for Hartree, xc for exchange correlation)

$$V(r) = -\frac{2Z}{r} + V_H(r) + V_{\mathrm{xc}}(r) \ , \tag{5a}$$

$$V_H(r) = \int |\mathbf{r} - \mathbf{r}'|^{-1} \rho(r') d\mathbf{r}' \ , \tag{5b}$$

$$V_{\mathrm{xc}}(r) = -4(3/8\pi)^{1/3} \rho(r)^{1/3} \beta(r) \ , \tag{5c}$$

where $\rho(r)$ is the electronic charge density. The exchange-correlation potential $V_{\mathrm{xc}}(r)$ is calculated in the local-density approximation (LDA).[26,27] $\beta(r)$ is a correlation function which interpolates between the high-density [small r; $\beta(r) \approx 1$] and low-density [large r; $\beta(r) \approx 1.5$–2] regions. The resulting potential $V(r)$ has no long-range

Coulomb tail and scatters like a neutral atom at large distances.[27] The asymptotic form of the incident and scattered wave functions therefore have the form

$$u_{kl}(r)\rightarrow \begin{cases} (1/kr)\sin(kr-l\pi/2+\delta_l) & \text{(distorting atomic potential)} \quad (6a) \\ j_l(kr) & \text{when } \delta_l\rightarrow 0 \\ & \text{(no potential; free electrons)} . \quad (6b) \end{cases}$$

In the core region, the LDA potential is strongly attractive, and suitable for calculating the target wave functions. The Schrödinger equation (4) and potential (5) have therefore also been used for calculating the ground-state and excited-state bound one-electron wave functions $u_i(r)$ and $u_n(r)$ (normalized to unity over the atomic volume). This provides localized corelike ground- and excited-state one-electron orbitals (3*d*, 4*d*, and 4*f* in La; 4*d*, 5*d*, and 5*f* in Th).

The LDA potential includes local correlation between the incident (scattered) electron and the core and valence electrons in the atomic volume. However, the LDA does not include long-range polarization, of van der Waals type, which is fine since we treat core excitation inside a metal, not in a free atom.

B. Independent-particle picture; unresolved angular momenta of the final states

After partial-wave expansion and integration over directions of the wave vector $\mathbf{k}'$ of the scattered electron, the angle-integrated differential cross section may be written as ($\omega=E-E'$ is the loss energy)

$$d\sigma_{ni}(E;\omega)/d\omega=\sigma_{ni}\delta(\omega_{ni}-\omega) , \quad (7)$$

$$\sigma_{ni}=32\pi(E'/E)^{1/2}\sum_{l,l'}\left[\sum_K(2K+1)^{-1}|\langle E'l',nl_n\|v^K\|El,il_i\rangle|^2+\sum_{K'}(2K'+1)^{-1}|\langle nl_n,E'l'\|v^{K'}\|El,il_i\rangle|^2 - \sum_{K,K'}(-1)^{K+K'}\begin{Bmatrix} l & K & l' \\ l_n & K' & l_i \end{Bmatrix}\langle E'l',nl_n\|v^K\|El,il_i\rangle\langle nl_n,E'l'\|v^{K'}\|El,il_i\rangle\right] . \quad (8)$$

The reduced matrix element is defined as

$$\langle a,b\|v^K\|c,d\rangle=[(2l_a+1)(2l_b+1)(2l_c+1)(2l_d+1)]^{1/2}\begin{bmatrix} l_a & K & l_c \\ 0 & 0 & 0 \end{bmatrix}\begin{bmatrix} l_b & K & l_d \\ 0 & 0 & 0 \end{bmatrix}R^K(a,b;c,d) \quad (9)$$

in terms of the Slater integral

$$R^K(a,b;c,d)=\int\int u_n(r_1)u_n(r_2)\frac{r_<^K}{r_>^{K+1}} \times u_n(r_1)u_n(r_2)dr_1\,dr_2 . \quad (10)$$

Equations (7) and (8) represent the inelastic differential cross section for transitions between *configurations*. Since it does not correspond to physical final states it cannot describe any particular loss line but rather corresponds to the sum of the lines associated with a particular configuration. This level of approximation is only useful if the exchange scattering is negligible, as, for example, for $E\geq 500$ eV the EELS in Figs. 1 and 2, which are dominated by the broad $4\underline{d}4f\ ^1P$ giant dipole continuum resonance around $\omega=117$ eV.

C. Resolved final states in *LS* coupling

In order to calculate the intensity of observed spectral lines, one must consider transitions to states characterized by all the relevant quantum numbers of the many-electron system.

In this paper we shall only consider transitions between pure *LS* levels of the target. The differential cross section for transitions of the target from the closed-shell ^1S ground state to $(\underline{in})^{2S+1}L$ final states, with scattering of the projectile between angular momentum states $lm\rightarrow l'm'$ and spin projections $\sigma\rightarrow\sigma'$, may be written as

$$d\sigma^{LS}_{\sigma'\sigma}(\omega;E)/d\omega=\sigma^{LS}_{\sigma'\sigma}\delta(\omega^{LS}_{ni}-\omega) , \quad (11)$$

$$\sigma^{LS}_{\sigma'\sigma}=16\pi(E'/E)^{1/2}\sum_{l',l,M_S}\begin{bmatrix} \frac{1}{2} & S & \frac{1}{2} \\ \sigma' & M_S & \sigma \end{bmatrix}^2|f^{LS}_{l'l}-g^{LS}_{l'l}|^2 , \quad (12)$$

where the direct ($f^{LS}_{l'l}$) and exchange ($g^{LS}_{l'l}$) amplitudes are given by

$$f^{LS}_{l'l}=\delta_{S,0}(2L+1)^{-1/2}\langle E'l',nl_n\|v^L\|El,il_i\rangle , \quad (13a)$$

$$g^{LS}_{l'l}=[(2L+1)(2S+1)]^{1/2}\sum_K(-1)^{L+K}\begin{Bmatrix} l & L & l' \\ l_n & K & l_i \end{Bmatrix} \times\langle nl_n,E'l'\|v^K\|El,il_i\rangle . \quad (13b)$$

If we do not observe the spin directions of the incident and scattered electrons we also have to sum over the final-state spin σ' (and average over the initial-state spin σ) in Eq. (12), with the result

$$\sigma^{LS}=16\pi(E'/E)^{1/2}\sum_{l',l}\tfrac{1}{2}|f^{LS}_{l'l}-g^{LS}_{l'l}|^2 \quad (14)$$

or written out in full,

$$\sigma^{LS}=8\pi(E'/E)^{1/2}(2L+1)(2S+1)$$
$$\times\sum_{l',l}\left|\delta_{S,0}\frac{2}{2L+1}\langle E'l',nl_n\|v^L\|El,il_i\rangle-\sum_K(-1)^{L+K}\begin{Bmatrix} l & L & l' \\ l_n & K & l_i\end{Bmatrix}\langle nl_n,E'l'\|v^K\|El,il_i\rangle\right|^2 . \quad (15)$$

At high impact energies the direct process will dominate, and we may consider the direct-only (DWD) cross section ($J=L;S=0$)

$$\sigma^{LS}=\sigma_d^L=32\pi(E'/E)^{1/2}\delta_{S,0}(2L+1)^{-1}\sum_{l',l}|\langle E'l',nl_n\|v^L\|El,il_i\rangle|^2 \quad (16)$$
$$=\delta_{S,0}(E'/E)^{1/2}\sum_{l,l'}A_{ll'L}[R^L(E'l',nl_n;El,il_i)]^2 , \quad (17)$$

where

$$A_{ll'K}=16\pi N_i(2l_n+1)(2l'+1)(2l+1)(2K+1)^{-1}$$
$$\times\begin{bmatrix} l' & K & l \\ 0 & 0 & 0\end{bmatrix}^2\begin{bmatrix} l_n & K & l_i \\ 0 & 0 & 0\end{bmatrix}^2 . \quad (18)$$

N_i is the number of initial-state electrons [$=2(2l_i+1)$ for the full shell].

We may also consider the LS-resolved exchange-only cross section

$$\sigma_x^{LS}=8\pi(E'/E)^{1/2}(2L+1)(2S+1)$$
$$\times\sum_{l',l}\left|\sum_K(-1)^{L+K}\begin{Bmatrix} l & L & l' \\ l_n & K & l_i\end{Bmatrix}\times\langle nl_n,E'l'\|v^K\|El,il_i\rangle\right|^2 . \quad (19)$$

In a first approximation, this should give a good description of those low-energy loss structures (Fig. 2) which have no direct contributions and which vanish already at low-to-intermediate impact energies (this excludes, e.g., the ^3P and ^3D levels in Fig. 2). The exchange-only cross section σ_x^{LS} in Eq. (19) is proportional to the multiplicity $(2L+1)(2S+1)$ of the final state but also depends on a state- and energy-dependent transition-matrix element.

Summing over all LS terms one obtains the distorted-wave exchange-only (DWX) cross section

$$\sigma_x=(E'/E)^{1/2}\sum_{l,l',K}B_{ll'K}[R^K(nl_n,El;E'l',il_i)]^2 , \quad (20)$$

where

$$B_{ll'K}=A_{ll'K}(l'\leftrightarrow l_n) . \quad (21)$$

The DWX cross section should give a reasonable description of the *total weight* of the exchange-driven low-energy-loss structures (in, e.g., Fig. 2).

D. Ionization

The ionization cross section is obtained from the EELS cross section by integrating over all losses leading to ionization of the target. Summing Eq. (7) over occupied (i) and empty (n) levels, and rewriting it in terms of a continuum final state of the target, normalized to unit current, one obtains the EELS spectrum

$$d\sigma(E)/d\omega=\sum_i\int d\varepsilon\,\sigma_{\varepsilon i}(E)\delta(\varepsilon-\varepsilon_i-\omega) . \quad (22)$$

The ionization cross section is then found by integrating the EELS for loss energies $\omega>|\varepsilon_i|$,

$$\sigma_{\text{ion}}(E)=\sum_i\int_0^{\omega/2}d\varepsilon\,\sigma_{\varepsilon i}(E) . \quad (23)$$

The factor of $\frac{1}{2}$ in the upper integration limit arises from the fact that the scattered and ejected continuum electrons are indistinguishable: We use the definition that the electron with the lowest kinetic energy is the ejected one.[42] Due to the unknown phase relation between the two outgoing continuum waves we are restricted to the maximum-interference approximation in order to avoid possible unphysical negative contributions to the cross section (see, e.g., Refs. 39 and 43).

E. Comments on spin-polarized EELS

In most EELS experiments (like Figs. 1–4) information about spin-triplet levels has to be deduced from the positions of loss lines and dependence of loss intensities on incident energy E. However, triplet excitations are also associated with spin-flip scattering, which could be detected if *spin-polarized* EELS were to be used.

With spin-polarized EELS the spin of the incident electrons is oriented along a given direction [spin up ($\uparrow$)] and one measures the spin projection ($\uparrow,\downarrow$) of the scattered electron. The spin polarization is defined as

$$P_{LS}=\frac{\sigma_{\uparrow\uparrow}^{LS}-\sigma_{\downarrow\uparrow}^{LS}}{\sigma_{\uparrow\uparrow}^{LS}+\sigma_{\downarrow\uparrow}^{LS}} . \quad (24)$$

In the case of no spin flips ($\sigma_{\downarrow\uparrow}^{LS}=0$) $P_{LS}=+1$. With equal number of spin-flip and no-spin-flip events ($\sigma_{\downarrow\uparrow}^{LS}=\sigma_{\uparrow\uparrow}^{LS}$) $P_{LS}=0$. With every event a spin flip ($\sigma_{\uparrow\uparrow}^{LS}=0$) $P_{LS}=-1$. Inserting the expression for the spin-dependent inelastic-scattering cross section from Eq. (14), one obtains

$$P_{LS}=2\sum_{M_S}\left[\begin{bmatrix}\frac{1}{2} & S & \frac{1}{2} \\ -\frac{1}{2} & M_S & \frac{1}{2}\end{bmatrix}^2-\begin{bmatrix}\frac{1}{2} & S & \frac{1}{2} \\ \frac{1}{2} & M_S & \frac{1}{2}\end{bmatrix}^2\right] \quad (25)$$

or

$$P_{L0}=+1 \quad (^1L;\text{no spin flip}) , \quad (26a)$$
$$P_{L1}=-\tfrac{1}{3} \quad (^3L;\tfrac{2}{3}\text{ spin flip},\tfrac{1}{3}\text{ no spin flip}) . \quad (26b)$$

In the absence of spin-orbit interaction, the spin polarization is independent of the orbital angular momentum L, and assumes fixed, energy-independent values for the different S values.

F. Comments on wave functions of *LS*-resolved states

In this paper we only consider single excited configurations (*in*) [Eqs. (2) and (3)] described by LDA independent-electron wave functions. All the LS terms involve the same wave functions and only differ by their LS-dependent energies and transition-matrix elements. We make a further simplification by neglecting the LS-dependent energy splittings when calculating cross sections. This means that the final energy $E'=E-\omega_{ni}^{LS}$ in Eqs. (14) and (15) is calculated as $E'=E-\omega_{ni}$. The approximation is good as long as the final energy E' is much larger than the LS term-level splitting. In the case of La $4\underline{d}4f$ and Th $5\underline{d}5f$ transitions, the width of the multiplet is about 15 eV, which means that there will be important differences in the kinematic $(E'/E)^{1/2}$ factor for $E' \leq 50-100$ eV.

There are a few things to be said about the $4\underline{d}4f\,{}^1P$ and $5\underline{d}5f\,{}^1P$ giant dipole resonances. Due to the large multiplet splitting, these resonances become $4\underline{d}\varepsilon f\,{}^1P$ and $5\underline{d}\varepsilon f\,{}^1P$ continuum resonances and should appear in calculations of *ionization,* rather than excitation, cross sections. To accomplish this one could calculate the transition amplitude within the random-phase approximation (RPA),[40] or use LS-dependent final-state wave functions and include ground-state correlations (initial- and final-state configuration interaction).[38] As mentioned above, we have not treated these aspects in this work. However, a few general observations may be appropriate.

The amplitude for *direct* inelastic scattering with $\mathbf{k}\rightarrow\mathbf{k}'$ and $i\rightarrow n$ may be written in the form

$$f_{\mathbf{k}'\mathbf{k}}=\langle \mathbf{k}',n\,|\,V_d(\mathbf{r}_1,\mathbf{r}_2;\omega)|\mathbf{k},i\rangle\ , \tag{27}$$

where $V_d(\mathbf{r},\mathbf{r}_2;\omega)$ represents an effective electron-electron interaction which depends on the energy transfer $\omega=E_{\mathbf{k}}-E_{\mathbf{k}'}=\varepsilon_n-\varepsilon_i$, and which is given by an RPA-type of integral equation.[2,3,27] In this way many-electron effects (including construction of LS levels) are dumped into an effective interaction, and the scattering states are treated as independent-electron states.

In the same way, the corresponding *exchange* amplitude with $\mathbf{k}\rightarrow n$ and $i\rightarrow\mathbf{k}'$ may be written as

$$g_{\mathbf{k}'\mathbf{k}}=\langle n,\mathbf{k}'\,|\,V_x(\mathbf{r}_1,\mathbf{r}_2;\omega')|\mathbf{k},i\rangle\ , \tag{28}$$

where again $V_x(\mathbf{r}_1,\mathbf{r}_2;\omega')$ represents an effective electron-electron interaction with $\omega'=E_{\mathbf{k}}-\varepsilon_n=E_{\mathbf{k}'}-\varepsilon_i$.

Note that screening and correlation effects act differently between the effective direct and exchange interactions since the energy transfer is constant (proportional to the energy loss $\omega=\varepsilon_n-\varepsilon_i$) for the direct process while it is proportional to the incident energy ($\omega'=E_{\mathbf{k}}-\varepsilon_n$) for the exchange process. For large incident energies the exchange interaction will therefore become unscreened, $V_x(\mathbf{r}_1,\mathbf{r}_2;\omega')\rightarrow 1/r_{12}$.

III. NUMERICAL RESULTS FOR CROSS SECTIONS OF LOSS PEAKS

A. General discussion

Figures 6–10 present numerical results, in the independent-particle approximation (LDA), for d-f and f-f excitation cross sections of La and Th at low-to-intermediate energies of the incident electron. Some of the *LS-unresolved* results have been briefly described in Ref. 25, while the LS-resolved results are all new.

The Born approximation has been calculated in two ways (see the Appendix). (i) In the momentum transfer ($\mathbf{q}$) formulation by calculating the m-averaged dynamic structure factor (BA). This provides the high-energy limit with forward scattering and dipole excitation. (ii) Using only the Kth component of the partial-wave expansion of the $\exp(i\mathbf{q}\cdot\mathbf{r})$ operator, corresponding to a definite angular momentum transfer K [BA (K)].

Moreover, we have evaluated the direct scattering

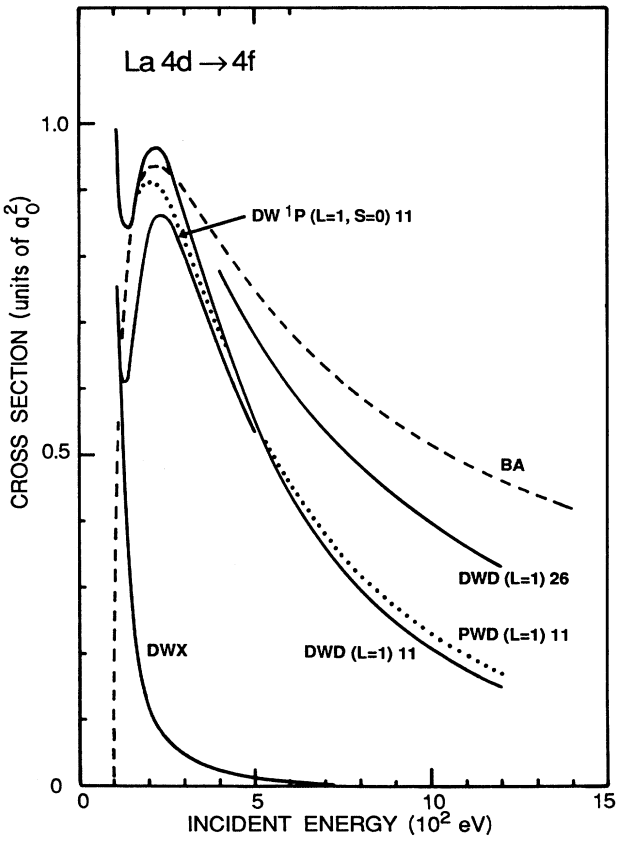

FIG. 6. Theoretical cross sections for electron-impact excitation of La $4d\rightarrow 4f$ transitions. BA, Born approximation; DW ^{2S+1}L, distorted-wave approximation, excitation of LS-term level; DWD, distorted-wave approximation, direct process; DWX, distorted-wave approximation, exchange process; PWD, plane-wave approximation, direct process. The notation DWD ($L=1$) 26 implies orbital angular momentum transfer $L=1$ and that 26 angular momenta, $l=0$–25, were used in the basis-function expansion.

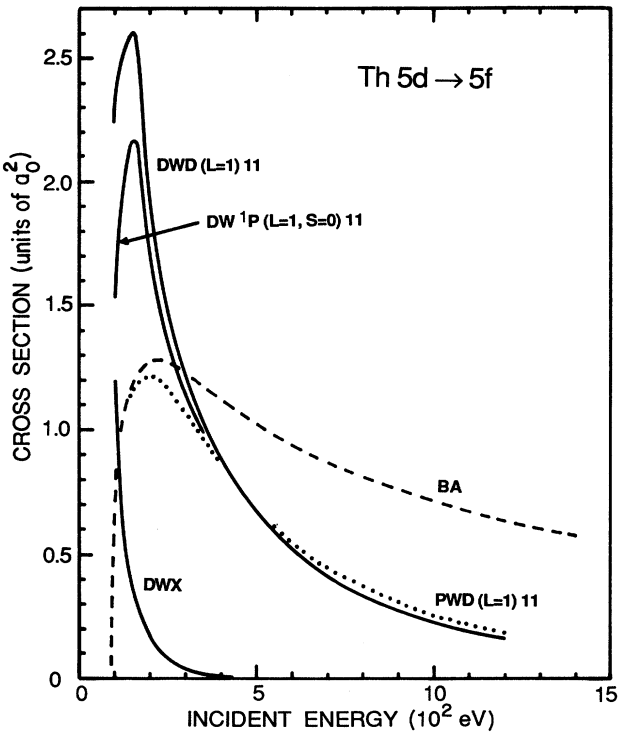

FIG. 7. Theoretical cross sections for electron-impact excitation of Th $5d \rightarrow 5f$ transitions. Notations as in Fig. 6.

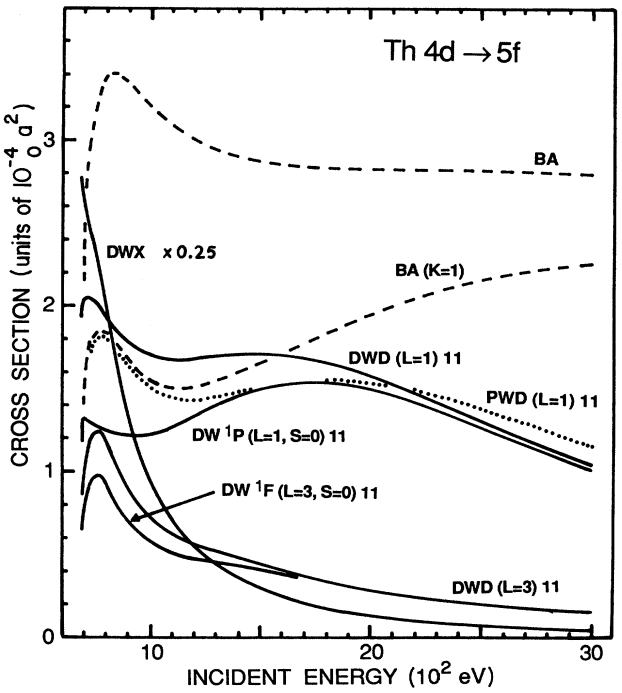

FIG. 9. Theoretical cross sections for electron-impact excitation of Th $4d \rightarrow 5f$ transitions. BA ($K=1$) implies that the dipole part of the $\exp(i\mathbf{q}\cdot\mathbf{r})$ transition operator has been used (see the Appendix). Otherwise notations as in Fig. 6.

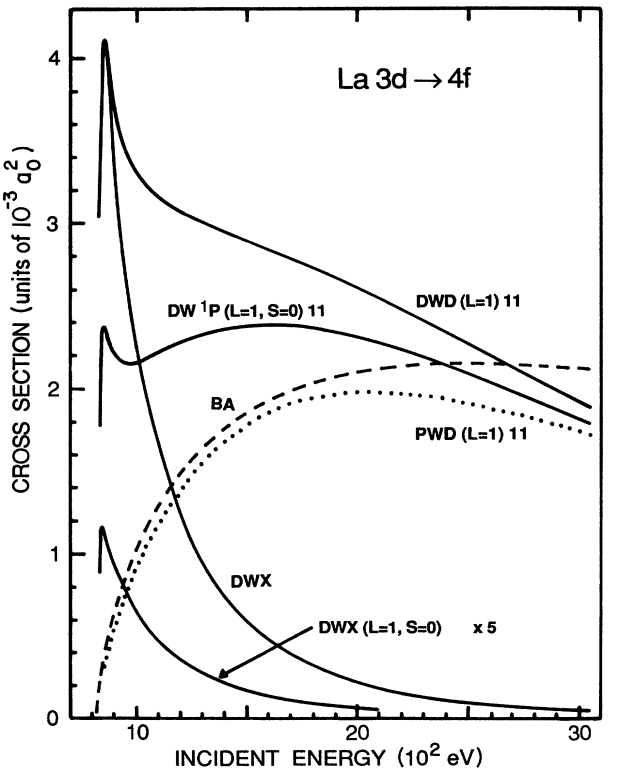

FIG. 8. Theoretical cross sections for electron-impact excitation of La $3d \rightarrow 4f$ transitions. Notations as in Fig. 6.

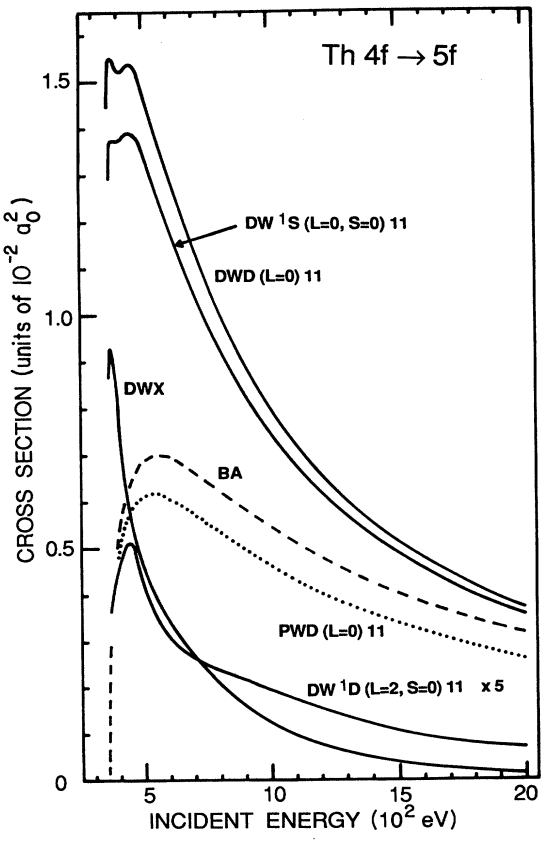

FIG. 10. Theoretical cross sections for electron-impact excitation of Th $4f \rightarrow 5f$ transitions. Notations as in Fig. 6.

$L=1$ cross section using the partial-wave expansion with zero scattering potential [plane-wave direct (PWD)]. The result should be close to the BA ($K=1$) and provide a check of the convergence of the partial-wave expansion. As seen, e.g., in Fig. 6, with 11 partial waves ($l,l' \leq 10$) in the expansion, the agreement is good at low energies but rapidly deteriorates at higher energies. With 26 partial waves there is considerable improvement at higher energies, but the expansion is clearly slowly convergent. For the distorted-wave exchange-only (DWX) cross section, however, we find a rapid convergence with respect to K, allowing truncation at $K \leq 3$ (since the continuum wave functions overlap localized d- and f-core electrons).

We shall not try to improve the convergence: instead we shall focus on the deviations between the partial-wave expansion with (DWD) and without (PWD) scattering potential, for the same number of partial waves. The difference should be a good measure of the effect of the core potential, since the PWD ($L=1$) represents the high-energy limit of the DWD ($L=1$) cross sections.

We now proceed to discuss the direct and exchange cross sections in Figs. 6–10 in some detail.

B. La $4d \rightarrow f$ transitions, Fig. 6

In the case of the $4\underline{d}4f$ lines in Figs. 1–3, the gross picture is given by the Russel-Saunders (LS) coupling scheme (the triplet-singlet splitting is ≈ 15 eV and the $4d$ spin-orbit splitting is ≈ 2 eV), even though in the 97–106-eV region there is considerable mixing due to spin-orbit interaction.

Comparison of the EELS and XPS spectra show that the $4\underline{d}4f$ excitations in the 97–106-eV range are nearly *localized* and only *weakly hybridized* with the conduction band: the $4f$-screened $4d$-hole levels appear as weak shake-down structures, meaning that $4f$ orbitals are not easily filled when pulled down below the Fermi level by the core-hole potential.

Since the physical $4\underline{d}f\ ^1P$ giant dipole resonance is broad and extends to, say, 140 eV, the DW $4\underline{d}4f\ ^1P$ cross section refers to the integrated intensity of the continuum $4d\varepsilon f\ ^1P$ giant dipole resonance, and is therefore only meaningful for incident energies E well above threshold, say $E > 1.5$–2 t.u. (threshold unit, E/ω_{ni}) (150–200 eV). For a correct description, we must work with a continuum (ionization) EELS formulation, as indicated in Secs. II D and II F.

The difference between the DWA and BA in Fig. 6 occurs mainly below the BA maximum, within 25 eV from threshold. There, however, the difference is huge due to the influence of the core potential. Note that this threshold behavior is due only to the effect of the static ground-state core potential on the incident and scattered electrons. We have not included any effects of the excitation (final-state potential, polarization) which can be expected to be important very close to threshold.

The effect on the cross section of including exchange is considerable, although only a very small part of the DWX amplitude interferes with the DWD ($L=1$) amplitude.

In Fig. 2, the EELS with $E_{\text{final}}(E')=1500$ eV provides an important reference. At the incident energy $E \geq 1000$ eV (10 t.u.), Fig. 6 shows that at this energy the exchange contribution (σ_x) is negligible. Therefore, the observable structure in the experimental EELS with $E'=1500$ eV in Fig. 2 must be due to the direct inelastic process and connected with ($\underline{d}f$) excitations with total angular momentum $J=1,3,5$ (angular momentum transfer $K=1,3,5$ from a $^1S_0$ ground state), as discussed by Netzer, Strasser, and Matthew.[4]

In the absence of spin-orbit interaction only $^1H_5$, $^1F_3$, and $^1P_1$ excitations are allowed. With spin-orbit interaction, all combinations of L and S leading to $J=1,3,5$ can be excited, i.e.,

$$\begin{aligned} &^1P_1 \rightarrow {}^3P_1, {}^3D_1, {}^1P_1\ , \\ &^1F_3 \rightarrow {}^3P_3, {}^1G_3, {}^1F_3\ , \\ &^1H_5 \rightarrow {}^3H_5, {}^3G_5, {}^1H_5\ . \end{aligned} \tag{29}$$

The experimentally observed peak positions agree very well with the calculated[6] positions of all of the $J=1,3,5$ levels in the bar diagram in Fig. 2. This is the basis for the tentative classification of the structure in the $E'=1500$ eV EELS in Fig. 2.

With this classification one finds that around $E'=600$ eV ($E \approx 7$ t.u.) the exchange-driven excitations are as important as many of the weaker excitations driven by the direct process. This is in agreement with the calculation (Fig. 6) which shows that the exchange cross section begins to be significant around $E=700$ eV (7 t.u.).

The $J=1,3,5$ levels should be more or less sensitive to interference effects between direct and exchange contributions, which means that the energy dependence of the intensities may not vary monotonically. On the other hand, the $J=2,4,6$ levels can be excited only via the exchange process (provided spherical symmetry holds for the ionic core in the solid), and the associated peaks in Figs. 1–3 seem to grow monotonically and rapidly with decreasing energy.

At very low incident energies the exchange contribution will be very important. The LS-resolved exchange-only cross section is given by σ_x^{LS} in Eq. (19). Apart from the statistical weight factor $(2L+1)(2S+1)$, the cross section depends on the incident (E) and final (E') energies through the angular and radial dependence of the transition matrix element.

The theoretical bar diagrams[6] in Figs. 1, 2, and 4 represent the statistical weights of the exchange-only cross section. The question is to what extent these statistical intensities are relevant for the experimentally observed EELS at very low energies. In Table I we present LS-resolved cross sections σ^{LS} [Eq. (14)] for the La $4\underline{d}4f\ ^{2S+1}L$ levels at a fairly low incident energy, $E=2$ t.u. (199.1 eV). According to these results, a statistical approximation (unity everywhere in the third column) needs to be corrected, because low angular momenta are favored. We think that this is at least qualitatively confirmed by the experimental results in Fig. 2 (in particular $E'=100$ eV), Fig. 3, and Refs. 13 and 14. In general, high-multiplicity G and H term levels do not seem to stand out in any way. In particular, the low-multiplicity $^3P_{0,1,2}$ levels around 97–98 eV are comparable in intensity to the high-multiplicity $^3H_{5,6}$ levels around 99.5 eV.

TABLE I. La $4\underline{d}4f$. Incident energy $E=2$ t.u. (199.1 eV). In the case of ^1P, ^1F, and ^1H levels, both direct and exchange contributions have been calculated. All other LS terms involve exchange-only results σ_x^{LS} from Eq. (19).

Term level	σ^{LS}/a_0^2	$\sigma_x^{LS}/(2L+1)(2S+1)$
^1P	0.842	
^3P	1.73×10^{-2}	1
^1D	5.73×10^{-3}	0.60
^3D	1.72×10^{-2}	0.60
^1F	1.89×10^{-2}	
^3F	1.68×10^{-2}	0.42
^1G	4.25×10^{-3}	0.25
^3G	1.27×10^{-2}	0.25
^1H	3.00×10^{-3}	
^3H	2.62×10^{-2}	0.41

Clark *et al.*[14] have recently analyzed the Ba $(4\underline{d}4f)^{2S+1}L_J$ multiplet structure in $YBa_2Cu_3O_7$ (from the EELS measurements by Ramsay, Netzer, and Matthew[13]) in terms of the statistical model, concluding that the excitation at low primary energies is *entirely* nonselective. This is of course true in the sense that there are no symmetry selection rules restricting the LS values of the $\underline{d}f$ configuration excited via the exchange process: all multiplet levels are allowed. The experimental results[13] for Ba do not differ significantly from the La results in Figs. 2 and 3, and the theoretical fit[14] accounts reasonably well for all multiplet levels but shows clear deviations from statistical weighting. We therefore conclude that the dynamics of the exchange process introduces a significant deviation from statistical weighting.

C. $5d \rightarrow f$ transitions, Fig. 7

In the case of the $5\underline{d}5f$ lines in Fig. 4, the coupling scheme is intermediate (the triplet-singlet splitting is ≈ 15 eV and the $5d$ spin-orbit splitting is ≈ 7 eV). This is demonstrated by the high intensity of the ^3D line at 89 eV in the "high-energy" EELS ($E_{\text{final}}=1200$ eV), which is dominated by the direct process and which resembles the photoabsorption cross section.[16] In the EELS with $E_{\text{final}}=100$ eV (Fig. 4), the exchange-driven loss lines appear in two groups separated by the $5d_{5/2}$-$5d_{3/2}$ spin-orbit interaction, in agreement with calculated positions.[6] In this case the Coulomb (exchange) interaction is not strong enough completely to redistribute the independent (statistical) electron excitations and spin-orbit split groups of levels appear.

Comparison of the EELS and XPS spectra (Fig. 4) show that the $5\underline{d}5f$ excitations in the 85–95-eV range are itinerant or strongly hybridized with itinerant states: The main $5d$ XPS peaks have the lowest binding energies and represent $5f$-well-screened hole levels (cf. Moser *et al.*[6] and Gunnarsson *et al.*[35]).

The Th $5d \rightarrow 5f$ cross sections in Fig. 7 differ significantly from La $4d \rightarrow 4f$. The influence of the atomic potential is very large already in the region of the maximum in the BA cross section, giving a very large difference between DWD and PWD cross sections in the 1–2-t.u. range.

Again, the $E_{\text{final}}(E')=1200$ eV EELS in Fig. 4 provides an important reference, essentially showing only directly excited $J=1,3,5$ levels (as identified from the bar diagram in Fig. 6 and Table I in Moser *et al.*[6]). The dominant lines are the $^3D_1$ and $^1P_1$ components of the giant dipole resonance, representing out-of-phase and in-phase oscillation of the spin-orbit split $5d_{5/2}$ and $5d_{3/2}$ shells.[2] There is also a trace of the $^3P_1$ line. The remaining weak structure should be due to $J=3,5$ nondipole *direct* transitions. For decreasing E', the exchange driven $J=2,4,6$ levels are the ones that grow most in relative intensity. In particular, we note the prominent appearance of the $^3P_{0,1,2}$ levels around 84–85.5 eV.

Table II shows the LS-resolved cross sections σ^{LS} [Eq. (14)] for the Th $5\underline{d}5f$ ^{2S+1}L levels at incident energy $E=2$ t.u. (175.8 eV). In this case the calculated deviations from statistical weighting are even more pronounced than in the La case. The experimental EELS with $E_{\text{final}}=100$ eV in Fig. 4 shows clear deviations from statistical weightings due to the direct $^3D_1$ transition around 90 eV plus direct $J=3,5$ direct transitions around 94 eV. Subtracting these features, the remaining EELS agrees qualitatively with the statistical spectrum. Beyond this, it is impossible to draw any firm conclusions.

The XPS spectrum in Fig. 4 can in principle serve as a reference: a major part of the relaxation processes involves filling of empty $5f$ screening orbitals, pulled down into the Fermi sea (FS) and coupled to the $5d$ core hole. The level population resulting from the FS$\rightarrow 5f$ charge-transfer screening process should be roughly statistical, which seems to be compatible with the XPS spectrum in Fig. 4. We note that the XPS shows strong similarities with the 100-eV EELS (if we "remove" the direct contributions discussed above). Again, beyond this it is impossible to draw any firm conclusions.

Finally it must be emphasized that for a quantitative comparison, calculations have to be J resolved from the beginning in order to properly account for interference effects between direct and exchange amplitudes.

TABLE II. Th $5\underline{d}5f$. Incident energy $E=2$ t.u. (175.8 eV). In the case of ^1P, ^1F, and ^1H levels, both direct and exchange contributions have been calculated. All other LS terms involve exchange-only results σ_x^{LS} from Eq. (19).

Term level	$\sigma^{LS}/(a_0^2)$	$\sigma_x^{LS}/(2L+1)(2S+1)$
^1P	1.94	
^3P	4.41×10^{-2}	1
^1D	1.53×10^{-2}	0.62
^3D	4.58×10^{-2}	0.62
^1F	3.56×10^{-2}	
^3F	3.78×10^{-2}	0.37
^1G	8.76×10^{-3}	0.20
^3G	2.63×10^{-2}	0.20
^1H	3.77×10^{-3}	
^3H	3.39×10^{-2}	0.21

D. La $3d \rightarrow 4f$ transitions, Fig. 8

The La $3d \rightarrow 4f$ EELS in Fig. 5 is clearly dominated by the $3d_{5/2}$-$3d_{3/2}$ spin-orbit interaction of ≈ 17 eV. Nevertheless, the $3d$-$4f$ exchange splitting is sufficiently large (≈ 5 eV) that the dipole-allowed $3\underline{d}_{5/2}4f(^3D)$ and $3\underline{d}_{3/2}4f(^1P)$ excitations will not be statistically 3:2 weighted (j-j limit): the intensities have to be calculated in intermediate coupling, and the weighting is instead approximately $3\underline{d}_{5/2}4f(^3D):3\underline{d}_{3/2}4f(^1P)=2:3$ (Ref. 2).

The maximum in the BA cross section occurs around 3 t.u., and the BA may be used from around 5 t.u. (because the PWD and DWD approximations give the same result). The difference between the DWA and BA occurs mainly below the maximum. There the difference is huge, however, due to the core potential.

Also, we find a very significant reduction of the direct $3\underline{d}4f\ ^1P$ cross section due to destructive interference with the exchange process.

The two experimental EELS curves in Fig. 5 represent rather low energies: Final energies $E'=600$ eV ($E\approx 0.8$ t.u.) and $E'=300$ eV ($E\approx 0.4$ t.u.). In threshold units this is as low as the lowest $4d$ EELS in Figs. 2 and 3. However, it is difficult to draw any firm conclusions by comparing the $4d$ and $3d$ spectra. The level structure in the low-energy part of the $3d$ EELS in Fig. 5 is not resolved (and maybe cannot be resolved). Possibly one may conclude that again the highest-multiplicity levels do not dominate the peak structures but rather contribute in a more modest way.

E. Th $4d \rightarrow 5f$ transitions, Fig. 9

The calculated excitation cross sections for the Th $4\underline{d}5f$ levels in Fig. 9 differ a lot from the corresponding La $3\underline{d}4f$ case.

The large difference compared with the La $3d \rightarrow 4f$ case arises from the nodal structure of the d and f wave functions. The DWD ($L=1$, $S=0$) cross section is low compared with La and the $L=3$ contribution is not negligible.

The inadequacy of the Born approximation (BA) in the low-energy region is apparent in Fig. 9. The reason is that the form-factor version of the BA (as defined here; see the Appendix) does not create excitations with definite angular momentum transfer L. The BA produces a mixture of angular momentum transfers, incompatible with a definite orbital angular momentum of target excited state. In Fig. 9 the large difference between the BA and the BA ($K=1$) cross sections [where the latter only makes use of the $K=1$ component of the multipole expansion of the $\exp(i\mathbf{q}\cdot\mathbf{r})$ operator] arises from the importance of the $K=3$ and higher odd components (see the Appendix). On the other hand, the dipole Born approximations BA ($K=1$) and PWD ($L=1$) are very similar (the difference is due to the limited number of high-l basis functions in the plane-wave expansion in PWD).

Finally we note that the DW $^1P_1$ and $^1F_3$ cross sections in Fig. 9 represent significant modifications of the direct (DWD) $^1P_1$ and $^1F_3$ cross sections due to exchange scattering.

F. Th $4f \rightarrow 5f$ transitions, Fig. 10

This transition is not optically allowed, and the cross sections fall quite rapidly with increasing energy of the incident electron.

The plane-wave expansion of the Born approximation (PWD) converges rapidly [the difference between the BA and PWD should be due to the unphysical superposition of transferred angular momenta in the BA in Eq. (A4)].

The effect of the potential is very large over a very wide energy region.

There are some experimental results[6,7] but the situation is complicated by the presence of (presumably) $4f \rightarrow 6d$ transitions of comparable strength. In future work, the $4f \rightarrow 5f$ and $4f \rightarrow 6d$ EELS should be treated together to provide a more severe test of the calculations.

G. La $3d \rightarrow \varepsilon f$ ionization, Figs. 11 and 12

As discussed in Secs. II F and III B, in the present work we do not properly describe the dipole oscillator strength distribution (final ^1P states) of the target. In the case of La ($n=4$) and Th ($n=5$) the $nd \rightarrow nf\ ^1P$ continuum giant dipole resonance[3] has been approximated within LDA (approximately equal to the configuration average Hartree-Fock (HF) discrete $d \rightarrow f$ line). In reality, most of the intensity in this transition should be pushed into a continuum ($n\underline{d}\varepsilon f\ ^1P$) resonance. The LDA basis $nd \rightarrow \varepsilon f$ continuum transitions alone are totally inadequate for describing $4d$ ionization in La and $5d$ ionization in Th.

In the case of the La $3d \rightarrow 4f$ and $3d \rightarrow \varepsilon f$ transitions the situation is different, however. The $3d \rightarrow \varepsilon f$ continuum transitions are only moderately modified by the polarization effects (RPA, HF ^1P), and the LDA basis continuum functions provide a reasonable first approximation.

In Fig. 11 we present $3d \rightarrow \varepsilon f$ continuum EELS of La for a sequence of incident electron energies. Figure 11 is directly relevant for the $3d \rightarrow \varepsilon f$ continuum part of the EELS above the $3d \rightarrow 4f$ loss peaks in Fig. 5 (in fact, the incident energies $E=1100$ and 1500 eV in Fig. 11 roughly correspond to the two spectra in Fig. 5). In future work, the $3d \rightarrow 4f$ EELS should be treated in a continuum rep-

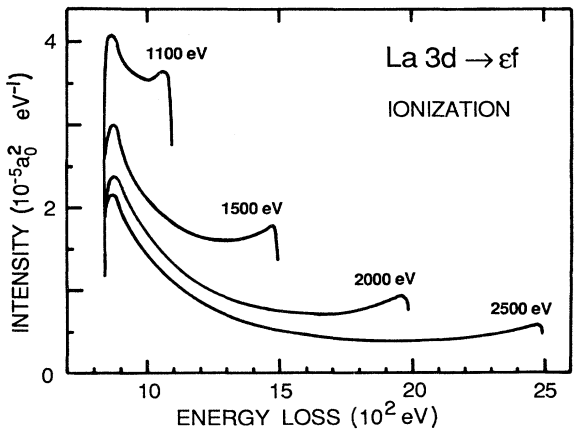

FIG. 11. Theoretical continuum EELS describing electron-impact ionization of La via $3d \rightarrow \varepsilon f$ transitions. Numbers labeling the curves indicate incident electron energies E.

resentation on equal footing with the $3d \rightarrow \varepsilon f$ EELS, like in photoabsorption calculations.[2]

Figure 12 shows the La $3d$ ionization cross section, obtained by integrating the EELS in Fig. 11 for fixed incident-electron energies. This cross section can directly be compared with the La DW ^1P $3d \rightarrow 4f$ cross section in Fig. 8. The result indicates that the cross sections for excitation and ionization become equal about 100 eV above threshold and that, in general, $3d \rightarrow \varepsilon f$ ionization is considerably more probable than $3d \rightarrow 4f$ excitation: in the region of the cross-section maxima around 2000 eV, the $3d$ ionization cross section is around four times larger than the $3d \rightarrow 4f$ excitation cross section.

Similar conclusions may been drawn from the photoabsorption cross section where about 75% of the $3d \rightarrow \varepsilon f$ oscillator strength resides in the continuum.[2]

IV. CROSS SECTION RATIOS. COMPARISON WITH EXPERIMENTAL RESULTS

A. General discussion

The present work is not yet at a stage where realistic EELS can be calculated for various incident-electron energies and directly compared with experimental spectra like the ones shown in Figs. 1–5. However, we have tried to make some rough comparisons between ratios of calculated cross sections and intensity ratios of experimental peaks in Figs. 1–5, e.g., experimental ratios like the ones in Fig. 1. In Figs. 1 and 2 the $4d4f$ $^1F_3$ peak at 105.3 eV is of particular importance as a reference peak because it remains isolated and well defined all the way from high to low incident-electron energies.

B. La $4d \rightarrow 4f$ ^3D to ^1F ratio, Fig. 13

The 101.7- and 105.3-eV loss peaks in Figs. 1 and 2 are very well defined at higher energies and can be traced to quite low energies; the intensity ratio of these lines should provide an important test of any calculation. The 105.3-eV peak is purely $^1F_3$. The 101.7 eV peak, however, is composite.

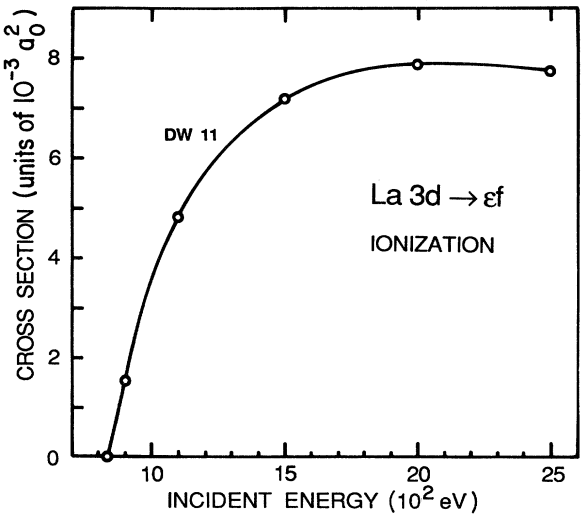

FIG. 12. Theoretical electron-impact ionization cross section of La via $3d \rightarrow \varepsilon f$ transitions, obtained by integrating the continuum EELS in Fig. 11 over loss energies. The results were obtained in the distorted-wave (DW) approximation with 11 partial waves, $l = 0-10$.

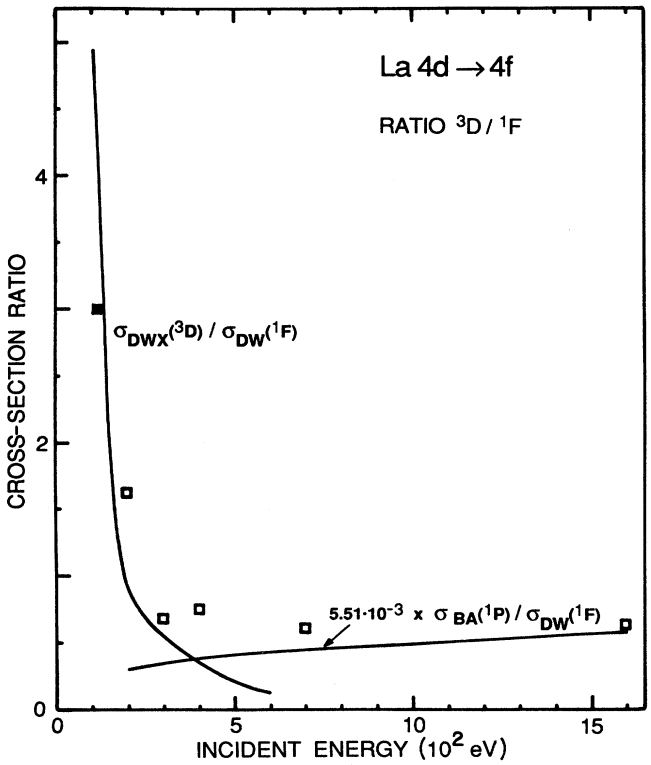

FIG. 13. Theoretical ^3D to ^1F ratios for La $4d \rightarrow 4f$ excitation (full curves) compared with estimates from experimental spectra (open squares, from Fig. 2; filled square from Fig. 3). The high-energy curve corresponds to $^3D_1$ to $^1F_3$. The low-energy curve includes all ^3D_J levels ($J = 1,2,3$).

(i) At high energies, the dipole excitation regime (XAS in Fig. 1), the 101.7 eV peak has purely $^3D_1$ character (and the $^1F_3$ peak has no intensity).

(ii) At intermediate energies (1500–3000 eV, Figs. 1 and 2) one can expect a nondipole singlet $^1H_5$ peak to grow up in parallel with (or at somewhat lower incident energies than) the $^1F_3$ peak; the $^1H_5$ peak should be several times smaller than the $^1F_3$ peak; the observed 101.7-eV peak should be a mixture of $^3D_1$ and $^1H_5$.

(iii) At low energies the peak will be a complicated mixture, mainly driven by the exchange scattering process.

For a rough comparison with experiments we have chosen to calculate a pure ^3D to ^1F ratio, shown in Fig. 13. This theoretical ratio is constructed in two ways.

(i) At *high* incident electron energies the $^3D_1$ (dipole-allowed) level derives its intensity from the $^1P_1$ resonance via spin-orbit coupling. We take the $^3D_1$ to $^1P_1$ ratio (5.51×10^{-3}) from Ref. 6. Furthermore, we assume that the Born approximation (BA) in Fig. 6 provides a good estimate of the $^1P_1$ cross section. As a consequence, a

reasonable high-energy estimate of the $^3D_1$ to $^1F_3$ ratio should be given by $5.51\times10^{-3}\ \sigma_{BA}(^1P_1)/\sigma_{DW}(^1F_3)$, which explains the right part of the curve in Fig. 13.

(ii) At sufficiently *low* incident-electron energies the ^3D excitation will essentially be exchange driven. We therefore calculate the distorted-wave exchange-only (DWX) cross section leading to ^3D (sum of $^3D_1$,$^3D_2$,$^3D_3$ contributions) and plot the ^3D to ^1F ratio. This explains the left part of the curve in Fig. 13.

In Fig. 13 we have also plotted values for the ratio of the experimental 101.7- and the 105.3-eV ($^1F_3$) peak intensities estimated from the spectra in Fig. 2. We would like to make the following comments.

(a) Intermediate-energy region (1500 eV): There is reasonable agreement between the experimental and theoretical ratios, which suggests that the 101.7-eV peak has mostly $^3D_1$ character. Further support for this conclusion can be found in Fig. 1. In the intermediate-energy region, a $^1H_5$ peak should roughly follow the energy variation of $^1F_3$ (increase relative to $^1P_1$) while a $^3D_1$ peak should follow $^1P_1$. From the 2920- to the 1600-eV EELS, the 105.3-eV peak increases strongly while the 101.7-eV peak remains roughly constant relative to $^1P_1$. We regard this as an indication of predominantly $^3D_1$ character of the 101.7-eV peak at these energies. Clark *et al.*[4] arrived at a similar conclusion in the case of Ba $4d\rightarrow4f$ in EELS for YBaCuO by calculating EELS intensities in intermediate coupling for the direct process in the Born approximation.[44]

This argument can be checked in still another way, by comparing the x-ray absorption spectrum (XAS) and the 2920-eV EELS in Fig. 1. As mentioned above, one would expect the $^3D_1$ XAS peak to reappear in the 2920-eV EELS with essentially the same strength relative to $^1P_1$. The problem is to determine the strength of the giant dipole resonances in the EELS (one of the major issues of this paper), because of the steeply varying background. If we assume that there is no additional background above the 4*d* limit and extrapolate the low-energy linear background into the $^1P_1$ region by a straight line, then we may conclude that all of the 101.7-eV intensity in the 2929-eV EELS may be ascribed to $^3D_1$. If instead we extrapolate to a horizontal background under the $^1P_1$ resonance, then around 70% may be ascribed to $^3D_1$.

(b) Low-energy region: There is again reasonable agreement between theory and experiment. However, we have no reason to associate the 101.7-eV peak with all of the *J* levels of $^3D_{1,2,3}$. According to Moser *et al.*[6] the 101.7-eV peak coincides with three levels with $J=1$, 3, and 5, and we identify these with $^3D_1$, $^3D_3$, and $^1H_5$. We may approximately remove the $^3D_2$ component by scaling the $^3D_{1,2,3}$ cross section by the statisitical weight $\frac{2}{3}$. Moreover, according to Table I, $\sigma^{LS}(^1H_5)$ is quite small around $E=200$ eV. Neglecting the $^1H_5$ component, this estimated $^3D_{1,3}$ cross section is still in reasonable agreement with experiment, in particular with the lowest-energy experimental point in Fig. 13, estimated from the 14 eV (final energy) EELS [Ref. 11(b)] in Fig. 3 (see also comment in Ref. 45).

From Fig. 3 we can in fact derive two more points with values around 3 and 4 for $E_{final}=15$ and 83 eV. This peaking seems to be due to the $^1F_3$ peak being relatively small at 83 eV final energy, which could in principle be due to an interference minimum for the $^1F_3$ level. Moreover, interference effects should be important for the $^3D_1$ and $^1H_5$ levels.

In general, matrix elements and interference effects are certainly expected to have an important influence on the cross sections of the individual LSJ transitions. Possibly the mixed nature of the EELS peaks may average out or mask some of the energy dependence. In any event, much improved calculations are necessary for drawing any more detailed conclusions. Moreover, the experimental points have large uncertainties due to overlapping structures and the identification of levels is far from clear. Interpretations therefore remain tentative.

C. La $4d\rightarrow4f$, Th $5d\rightarrow5f$ ^1F to ^1P ratio, Fig. 14

The $^1F_3$ to $^1P_1$ ratio is important because, as seen in Figs. 1 and 2, the ^1F loss peak is well defined while the ^1P peak is a broad continuum resonance. Theoretical knowledge of the ^1F to ^1P ratio will give information about the integrated intensity of the broad ^1P giant dipole resonance, which otherwise is difficult (or impossible) to isolate from the background. At sufficiently high energies we use the BA for the ^1P cross section, in order to achieve full convergence with respect to the partial wave expansion.

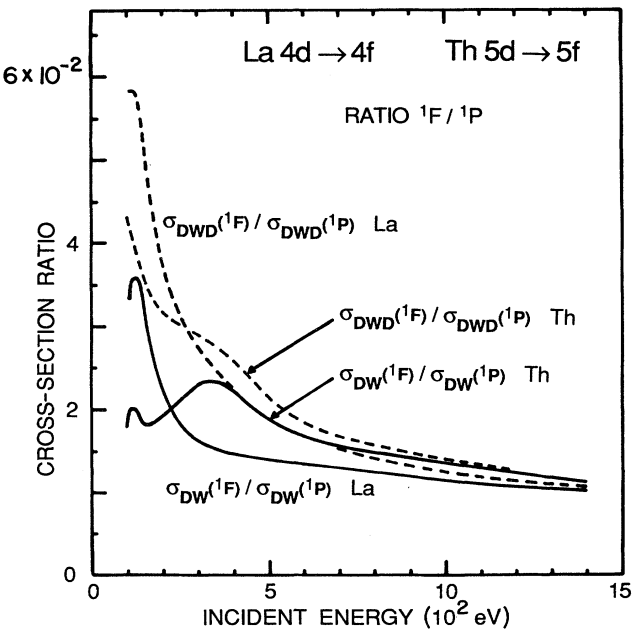

FIG. 14. Theoretical ^1F to ^1P ratios for La $4d\rightarrow4f$ excitation and Th $5d\rightarrow5f$ excitation. Dashed curves include only the direct process, full curves also include exchange.

The calculated $\sigma_{DW}(^1F)/\sigma_{DW}(^1P)$ ratio[46] in Fig. 14 decreases slowly and monotonically above $E=200$ eV incident energy, while the experimentally deduced ratio in Fig. 1 shows a pronounced maximum around $E=1000$ eV. *This seems like a clear disagreement between theory and experiment.* We would like to suggest that the problem is connected with the analysis of the experimental data. The ratios in the inset in Fig. 1 (Ref. 4) have been determined as ratios of peak heights (not peak areas); however, especially for low incident energies ($E=320-560$ eV), it is not evident how to determine the peak height of the ^1P continuum resonance relevant for determining its integrated intensity. With a different background subtraction, reducing the ^1P intensity at low energies, the ^1F to ^1P ratio will continue to increase below $E=1000$ eV, as suggested by the calculated ratio in Fig. 14 and by the dashed extrapolations in Fig. 1.

We may now also go back to Sec. IV A above, and compare with the ^3D to ^1P ratio in the inset of Fig. 1. To be consistent, we have to determine the experimental "^3D" to ^1P ratio with a reduced ^1P peak height for $E \leq 560$ eV. As a result, the corresponding data points (triangles) will be shifted upwards. The "^3D" to ^1P ratio is now roughly constant down to $E \approx 500$ eV, below which energy it begins to rise, finally following the steep exchange-only curve.

D. La ($3d, 4d$) Th ($4d, 5d$) total exchange to ^1P ratio, Fig. 15

In the La $3d \rightarrow 4f$ case the loss spectrum (Fig. 5) consists of well-defined peaks or groups of peaks which can be reasonably well separated from the background. Due to the large $3d$ spin-orbit splitting (17 eV), the EELS groups into structures based on $3d_{5/2} \rightarrow 4f$ and $3d_{3/2} \rightarrow 4f$ transitions. On the independent-particle level, the relative intensity of these groups will be statistically weighted, 3:2. Between these groups, there is, however, strong interaction between the dipole-allowed levels, leading to intensity reversal and to a ratio of 2:3 for the peaks observed in photoabsorption[2] (corresponding to intermediate coupling). On the other hand, for the exchange-driven structures there is very weak interaction between the $3d_{5/2}$ and $3d_{3/2}$ groups; the 3:2 intensity ratio should then still be reasonable. Therefore, we would expect the exchange-driven loss structure to be more important relative to the dipole-allowed peak in the $3d_{5/2} \rightarrow 4f$ region than in the $3d_{3/2} \rightarrow 4f$ region.

Figure 15 shows the calculated ratios of total exchange to ^1P cross sections $\sigma_{DWX}/\sigma_{DW}(^1P)$ ($\sigma_{DWX}=\sigma_X$ [Eq. (20)]) for all considered transitions, plotted versus incident energy E in threshold units. We note that in La the ratio approximately follows the same curve for the $3d \rightarrow 4f$ and $4d \rightarrow 4f$ transitions when the energy is measured in threshold units. Moreover, these ratios approach values around 1–2 at threshold. In the threshold region we can then expect the integrated "^3L" level structure and the ^1P dipole level to have comparable intensities, both in the $4d$ and $3d$ cases. In Th, the exchange to direct ratio for $5d \rightarrow 5f$ lies somewhat below the ratio for La, while the ratio for the $4d \rightarrow 5f$ case lies high above; in this representation the calculated difference between

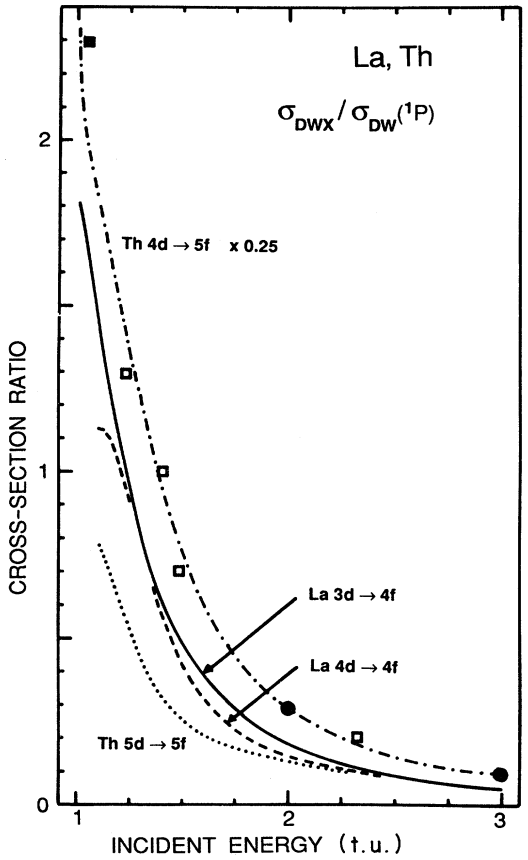

FIG. 15. Theoretical total exchange to ^1P ratios for La $4d \rightarrow 4f$ and $3d \rightarrow 4f$ excitation, and Th $5d \rightarrow 5f$ and $4d \rightarrow 5f$ excitation. Most of the data points (open and filled squares) have been derived from experimental spectra for La, like in Fig. 5, by estimating the ratio of intensities (area) of the low-energy to the high-energy structures (after summing contributions from the spin-orbit split components). Two data points (open circles) have been derived from the $4d \rightarrow 4f$ spectra in Fig. 2 by estimating the area of the low-energy structure, except the $^1F_3$ level, taking the ratio to the $^1F_3$ peak and using the calculated $^1F_3$ to ^1P ratio (Fig. 14) to obtain the "experimental" total exchange to ^1P ratio. □, La $3d \rightarrow 4f$, from Fig. 5 and H. R. Moser (unpublished). ■, La $3d \rightarrow 4f$, from Ref. 11. ●, La $4d \rightarrow 4f$, from Fig. 2 (t.u. is threshold units).

La and Th is clearly demonstrated.

Returning to the La $3d \rightarrow 4f$ experimental EELS, assuming statistical weighting (3:2) of the nondipole transitions and taking into account the nonstatistical ratio of the dipole transitions[2] we find that the nondipole to dipole allowed (exchange to direct) intensity ratio in the $3d_{5/2} \rightarrow 4f$ structure is about a factor of 2 larger than in the $3d_{3/2} \rightarrow 4f$ structure. This conclusion is independent of the incident energy and agrees well with experiment.[4–6]

In Fig. 15 are also shown data points estimated from experimental $3d \rightarrow 4f$ (Refs. 4, 6, and 11) and $4d \rightarrow 4f$ (Refs. 4 and 6) spectra. There is reasonable agreement between theory and experiment, especially regarding the energy dependence. The experimental ratio is about a

factor of 1.3 larger than theory. One explanation is that we have been using the LDA $4f$ wave function (roughly equivalent to the HF configuration average), instead of a $4f$ wave function properly coupled to the hole, $3d^{-1}4f\,{}^1P$. Using the RPA to describe the $3d^{-1}4f\,{}^1P$ excitation, part of the $3d^{-1}4f$ intensity will be pushed to the continuum and the exchange to ${}^1P$ ratio will increase. Differences might also be due to other approximations, e.g., local-density potential for incident and scattered electrons.

V. SUMMARY AND CONCLUDING REMARKS

The purpose of this work has been to study the intensity variation of electron-energy-loss spectra (EELS) for La and Th metal, involving $4d\rightarrow 4f$ and $3d\rightarrow 4f$ transitions in La and $5d\rightarrow 5f$ and $4d\rightarrow 5f$ transitions in Th, when the incident-electron energy is lowered from high energies down to threshold. Of particular interest has been the appearance at low incident-electron energies of new EELS structure[4–14] which can only be explained by excitation via exchange scattering, i.e., the incident electron becomes captured into an atomiclike f level and a core electron is knocked out.

Previous work[4–6,14] has calculated cross sections for direct excitation in the Born approximation (BA) and studied the appearance of nondipole loss features as well as discussed the breakdown of selection rules at low energies due to exchange scattering.[4,14] In the presence of a core hole, the f levels are essentially localized within the ion cores in the metal, and an atomic model for core$\rightarrow f$ transitions is therefore adequate for cross-section calculations (but not for the detailed behavior of the EELS as a function of loss energy for $5f$ electron systems; cf. photoionization of Th, Ref. 30).

In this paper we have tried to go a few steps further by resorting to approximations that should work at low energies and by explicitly considering exchange scattering. We have calculated LS-resolved cross sections for electron-impact excitation of core electrons to $4f$ levels in La and $5f$ levels in Th within the local-density approximation (LDA). We have used the distorted-wave approximation (DWA) at low energies and calculated both direct and exchange scattering processes. In addition we have also made use of the Born approximation in the whole energy range.

In general, our calculated LDA cross sections account rather well for the observed relative intensities of localized $d\rightarrow f$ excitations in EELS in La and The metal. This should provide a basis for deducing quantitative information about a variety of inelastic processes in rare-earth and actinide solids.

We would like to draw attention to a few specific results.

(i) In La, the $3d\rightarrow 4f$ and $4d\rightarrow 4f$ transitions show closely similar exchange-to-direct ratios as functions of incident-electron energy on the scale of the excitation energy. The ratio is of the order of unity at threshold. We find a clear difference between $4f$ and $5f$ elements in what concerns low-energy and threshold behavior. In particular, the $4d\rightarrow 5f$ transition in Th seems to be very special. Our calculated branching ratios for ${}^3L$ to ${}^1P$ and ${}^1F$ to ${}^1P$ are in reasonable agreement with experimental trends.

(ii) Our calculations show significant deviations from the qualitatively reasonable picture of statistical weighting[13,14] in the near-threshold region due to transition-matrix element effects. Experimental evidence for dynamic variation of the electron-energy-loss spectrum in the exchange-dominated low-incident-energy region[11] can be found in the La $4d$ EELS in Fig. 3.

Improvements necessary in the description of the inelastic-scattering process cannot be assessed before the description of the excitation process has been improved and until the present calculations have been further tested and extended. Necessary extensions will include the following.

(i) Spin-orbit interaction and description of the LSJ structure, and the resulting dependence of scattering cross sections on the total angular momentum J. This is absolutely necessary for any attempt at detailed comparison with experimental results. The LSJ levels are overlapping in the experimental EELS and can perhaps not be resolved. One must therefore theoretically reproduce the essential part of the experimental peak structure, and then calculate the relevant cross sections. Interference effects between exchange and direct scattering will affect different LSJ levels in different ways, which may be a useful source of further information.

(ii) Many-electron treatment of dielectric response and screening through the RPA or through corresponding parts of many-body perturbation theory. This will provide a good description of the dipole excitation spectrum which dominates at high excitation energies.

(iii) Continuum EELS treatment of BA, La $4d$-$4f$, and Th,U $5d$-$5f$ giant dipole resonances. In the present work, these resonances have been treated as discrete, localized excitations. In reality, they are $4d$-εf and $5d$-εf continuum resonances even in free atoms and have to be described within the framework of electron impact ionization.[38]

Finally, it should be emphasized that experiments with spin-polarized electrons are becoming increasingly important.[1(c),1(d),47–56] Recent work involves spin-polarized photoelectron diffraction,[48–50] spin-polarized photoemission,[51,52] spin-polarized secondary-electron emission,[53] spin-polarized inverse photoemission,[54] and spin-polarized EELS (SPEELS).[55,56] Many of these experiments study, for example, magnetic moments of transition metals and rare earths in thin films and at surfaces, which is of great theoretical interest.[57]

There has also been considerable theoretical work on interpretation of experimental SPEELS. For example, Penn and Apell[58] have recently analyzed experimental results[55] from low-energy inelastic electron scattering from Fe and concluded that exchange scattering involving Stoner excitations from the $3d$ and to free-electron states is surprisingly important.

To finish, we would like to point out that high-resolution SPEELS should provide an important tool for characterizing the $d^{10}({}^1S_0)\rightarrow d^9f({}^{2S+1}L_J)$ transitions in rare-earth and actinide solids.

In LS coupling, $P_{LSJ}=P_S=+1$ if $S=0$ and $-\frac{1}{3}$ if $S=1$, independent of L and of incident energy. All triplet levels have the same spin polarization. In intermediate coupling, with important effects of spin-orbit interaction, P_{LSJ} depends on J and will, in principle, show interference effects with excitation energy. By analyzing the variation of the spin polarization with loss energy across the level structures in Figs. 1–5, perhaps with application of external magnetic fields, one should be able to achieve some separation of overlapping structures.

High-resolution SPEELS on atomic rare-earth and actinide systems could provide very important references. Th $d^{10}(^1S_0) \rightarrow d^9 f(^{2S+1}L_J)$ transitions will be the same, but without hybridization. Instead, the dynamics of valence electrons may cause additional complications. With free atoms, one has the possibility to make angle-resolved experiments to determine the total orbital angular momentum L. Moreover, one can determine the energy dependence of excitation cross sections without influence of the electron mean free path in the solid.

ACKNOWLEDGMENTS

This work has been supported by a grant from the Swedish Natural Science Research Council.

APPENDIX: THE BORN APPROXIMATION

In this appendix we provide some details of our calculations in the Born approximation (BA). For an empty final-state shell, the BA cross section is given by

$$\sigma_{\mathrm{BA}}(E)=16\pi E^{-1}\int_{q_{\min}}^{q_{\max}} dq\, q^{-3}\sum_m |\langle n,m|e^{iq\cdot r}|i,m\rangle|^2 , \tag{A1}$$

$$q_{\max}=\sqrt{E}+\sqrt{(E-\omega_{ni})} , \tag{A2a}$$

$$q_{\min}=\sqrt{E}-\sqrt{(E-\omega_{ni})} . \tag{A2b}$$

m is the projection of the orbital angular momentum along the scattering vector q, giving the selection rule $\Delta m=0$. In the inelastic form factor

$$F_{ni}(\mathbf{q})=\langle n|\exp(i\mathbf{q}\cdot\mathbf{r})|i\rangle , \tag{A3}$$

the density operator may be expanded in multipoles,

$$F_{ni}(\mathbf{q})=\left\langle n\left|\sum_K i^K(2K+1)j_K(qr)P_K(\mathbf{q}\cdot\mathbf{r})\right|i\right\rangle . \tag{A4}$$

For $d \rightarrow f$ transitions, for example, the angular momentum transfer may take the values $K=1,3,5$. As a result, the form factor $F_{ni}(\mathbf{q})$ represents a definite momentum transfer $\mathbf{q}$ but a mixture of parities and angular momentum transfers. In the limit of high incident-electron energy small momentum transfers $\mathbf{q}$ will be favored: dipole excitations ($K=1$) will then dominate, and the BA will describe excitation with definite parity. At low energies, however, $E \approx \omega_{ni}$ and $q_{\max} \approx q_{\min} \approx \sqrt{E}$ [Eq. (3)]: the momentum transfer $\mathbf{q}$ will occur in a narrow window of rather large momenta, and a mixture of angular momentum transfers cannot be avoided.

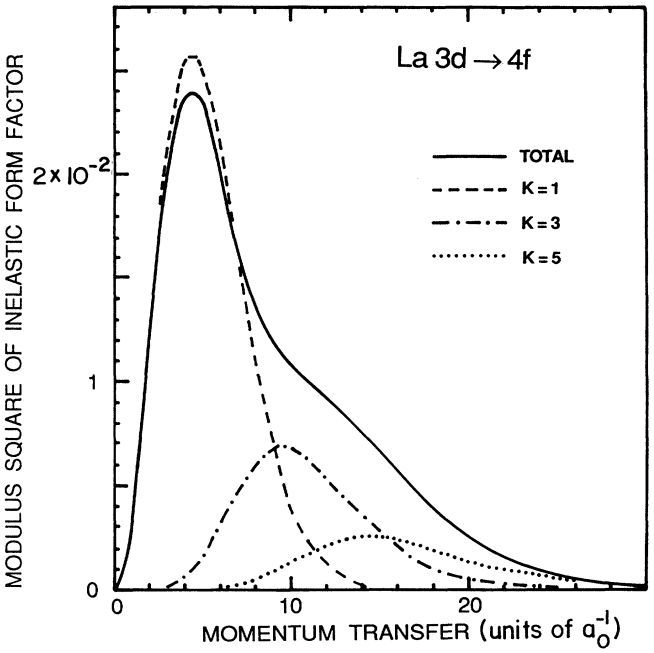

FIG. 16. m-averaged modulus square of the inelastic form factor for La $3d \rightarrow 4f$ transitions. Full curve refers to $|F_{ni}(\mathbf{q})|^2$, an essential part in the BA cross sections. Broken curves refer to the components $|F_{ni}^K(\mathbf{q})|^2$, entering the BA ($K=1$), BA ($K=3$), and BA ($K=5$) cross sections.

These considerations are illustrated in Figs. 16 and 17 for La $3d \rightarrow 4f$ and Th $4d \rightarrow 5f$ transitions, respectively. At the core-level thresholds, $q_{\max} \approx q_{\min} \approx \sqrt{E} \approx 5(a_0)^{-1}$. In the La $3d \rightarrow 4f$ case (Fig. 16), the $K=1$ dipole component dominates the q integration in Eq. (A1) even near threshold, and the BA cross section (Fig. 8) does not

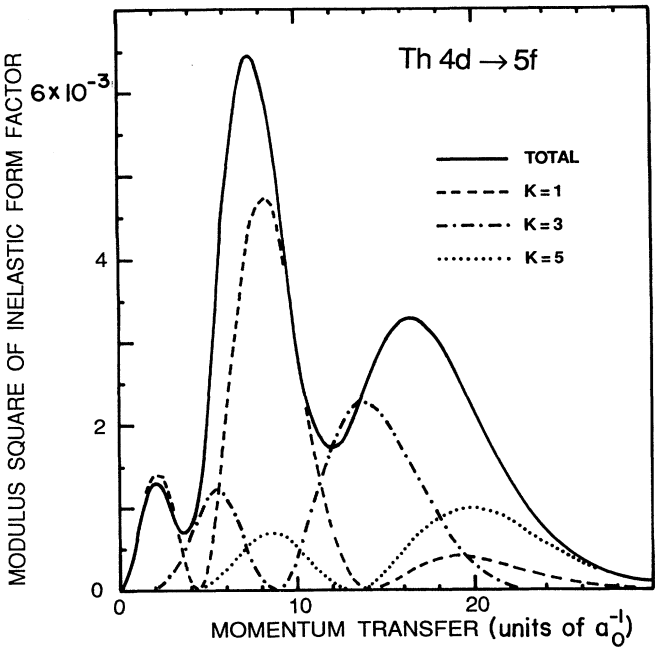

FIG. 17. m-averaged modulus square of the inelastic form factor for Th $4d \rightarrow 5f$ transitions (see caption to Fig. 16).

differ much from the $K=1$ plane-wave result, PWD ($K=1$)

The case of Th $4d \rightarrow 5f$ is quite different. Figure 17 shows that $K=1$ component only dominates for quite small momentum transfers. In the threshold region, with q peaking around $5(a_0)^{-1}$, $K=1$, and $K=3$ are equally important, and the BA differs very much from the plane-wave dipole PWD ($L=1$) result (Fig. 9).

The usual way to handle this problem in the Born approximation is to fix the angular momentum transfer L by including only the appropriate multipole component needed to excite the ${}^1S \rightarrow \underline{in}\ {}^1L$ transition with parity $(-1)^L$,

$$F_{ni}^K(q) = \langle n | i^K (2K+1) j_K(qr) P_K(\mathbf{q}\cdot\mathbf{r}) | i \rangle \delta_{L,K} \ . \quad \text{(A5)}$$

In the initial and final states, the atomic target and the electron projectile are separated in space, and the atomic states must be characterized by definite parity and the transitions by definite angular momentum transfer L.

As seen in Fig. 9, the BA ($K=1$) cross section is very close to the PWD ($L=1$) result (in the threshold region, where the PWD plane-wave expansion is well converged).

---

*Present address: Physik Institut der Universität Zürich, Schönberggasse 9, CH-8001 Zürich, Switzerland.

[1](a) H. Raether, *Excitation of Plasmons and Interband Transitions by Electrons,* Springer Tracts in Modern Physics Vol. 88 (Springer-Verlag, Berlin, 1980); (b) J. Kessler, *Polarized Electrons* (Springer-Verlag, Berlin, 1976); (c) *Polarized Electrons at Surfaces,* edited by J. Kirschner (Springer-Verlag, Berlin, 1985); (d) *Polarized Electrons in Surface Physics,* edited by R. Feder (World Scientific, Singapore, 1985); (e) M. Inokuti, Rev. Mod. Phys. **43**, 297 (1971); M. Inokuti, Y. Itikawa, and J. E. Turner, *ibid.* **50**, 23 (1978).

[2]G. Wendin, Phys. Rev. Lett. **53**, 724 (1984), and references cited therein.

[3]G. Wendin, in *Giant Resonances in Atoms, Molecules and Solids,* Vol. 151 of *NATO Advanced Study Institute, Series B: Physics,* edited by J.P. Connerade, J. M. Esteva, and R. C. Karnatak (Plenum, New York, 1987), and references cited therein.

[4]F. P. Netzer, G. Strasser, and J. A. D. Matthew, Phys. Rev. Lett. **51**, 211 (1983).

[5]J. A. D. Matthew, G. Strasser, and F. P. Netzer, Phys. Rev. B **27**, 5839 (1983).

[6]H. R. Moser, B. Delley, W. D. Schneider, and Y. Baer, Phys. Rev. B **29**, 2947 (1984).

[7]H. R. Moser, Ph.D. thesis, Zürich, 1983.

[8]J. Kanski and G. Wendin, Phys. Rev. B **24**, 4977 (1981).

[9]J. Kanski (private communication).

[10]J. Onsgaard, C. Jansson, and J. N. Andersen, J. Electron. Spectrosc. Relat. Phenom. **46**, 227 (1988).

[11](a) H. Hinkers, R. Stiller, and H. Merz, Phys. Rev. B **40**, 10 594 (1989); (b) H. Hinkers, Thesis, Universität Münster, 1989.

[12]A. Ando, K. Saiko, K. Ueno, and A. Koma, Jpn. J. Appl. Phys. **27**, L304 (1988).

[13]M. G. Ramsay, F. P. Netzer, and J. A. D. Matthew, Phys. Rev. B **39**, 732 (1989).

[14]C. W. Clark, J. A. D. Matthew, M. G. Ramsay, and F. P. Netzer, Phys. Rev. A **40**, 4902 (1989).

[15]M. Cukier, B. Gauthé, and C. Wehenkel, J. Phys. **41**, 603 (1980).

[16]Photoabsorption. La $4d$ region: P. Rabe, Doctoral thesis, Universität Hamburg, 1974; (unpublished); La $3d$ region: R. C. Karnatak, J.-M. Esteva, and J. P. Connerade, J. Phys. B **14**, 4727 (1981); Th $5d$ region: M. Cukier, P. Dhez, B. Gauthé, P. Jaeglé, C. Wehenkel, and F. Combet Farnoux, J. Phys. **39**, 48 (1978); **39**, L315 (1978).

[17]Photoemission and photoyield, Th metal: A. Fujimori and J. H. Weaver, Phys. Rev. B **31**, 6411 (1985); Photoyield and photodesorption, $YBa_2Cu_3O_7$: R. A. Rosenberg and C.-R. Wen, *ibid.* **37**, 5841 (1988); **37**, 9852 (1988).

[18]J. Kanski, P. O. Nilsson, and I. Curelaru, J. Phys. F **6**, 1073 (1976).

[19]R. J. Liefeld, A. F. Burr, and M. V. Chamberlain, Phys. Rev. A **9**, 316 (1974).

[20]F. Riehle, Doctoral thesis, Universität Karlsruhe, 1977; Jpn. J. Appl. Phys. **17**, 314 (1978).

[21](a) A. S. Shulakov, T. M. Zimkina, A. P. Braiko, V. I. Radchenko, and V. A. Fomichev, Fiz. Tverd. Tela (Leningrad) **25**, 789 (1983) [Sov. Phys. Solid State **25**, 451 (1983)]; (b) A. S. Shulakov, T. M. Zimkina, A. P. Braiko, and A. P. Stepanov, Opt. Spektrosk. **58**, 776 (1985) [Opt. Spectrosc. (USSR) **58**, 475 (1985)]; (c) A. S. Shulakov, T. M. Zimkina, and A. P. Stepanov, Fiz. Tverd. Tela (Leningrad) **27**, 112 (1985) [Sov. Phys. Solid State **27**, 65 (1985)].

[22]P. Motais, E. Belin, and C. Bonnelle, Phys. Rev. B **30**, 4399 (1984).

[23]J. K. Lang and Y. Baer, Phys. Rev. B **21**, 2060 (1980).

[24]G. Wendin, Phys. Rev. Lett. **39**, 48 (1977); K. Nuroh and G. Wendin, Phys. Rev. B **24**, 5533 (1981).

[25]H. R. Moser and G. Wendin, Solid State Commun. **65**, 107 (1988).

[26]*Theory of the Inhomogeneous Electron Gas,* edited by S. Lundqvist and N. H. March (Plenum, New York, 1983); see, e.g., the article by Williams and von Barth.

[27]Z. Crljen and G. Wendin, Phys. Scr. **32**, 359 (1985); Phys. Rev. A **35**, 1555 (1987); **35**, 1571 (1987).

[28]A. Zangwill and D. A. Libermann, Phys. Rev. B **36**, 6705 (1987).

[29]In the presence of core holes, $4f$ and $5f$ electrons resonate in the *inner* well of the $l=3$ double-well potential (Ref. 27). Calculations within an embedded-atom model (Ref. 30) show that the $4f$ level in Ba and La is practically unaffected by a metallic environment, while the $5f$ level in Th is slightly broadened by hybridization. A calculation (Ref. 30) of the photoionization cross section for an embedded Th atom (Th in jellium) within a local-density random-phase approximation gives good agreement with experiment [Fujimori and Weaver (Ref. 17)].

[30]G. Wendin and J. Luberek (unpublished).

[31]Metallic La and Th have closed-shell Xe-like ion cores and itinerant *s-p-d* conduction electrons. The ion cores therefore have ${}^1S$ ground states, and transitions are defined by only mentioning the final states.

[32]For further discussion of the character of the $4\underline{d}\varepsilon f\ {}^1P_1$ giant dipole resonance, see, e.g., G. Wendin, J. Phys. B **9**, L297 (1976); G. Wendin and A. F. Starace, *ibid.* **11**, 4119 (1978); ar-

ticles in Ref. 3, and references cited therein.
[33]G. Wendin, Struct. Bond. **45**, 1 (1981), and references cited therein.
[34]G. Wendin, in *X-ray and Atomic Inner-Shell Spectra,* edited by B. Crasemann, AIP Conf. Proc. No. 94 (AIP, New York, 1982), p. 495.
[35]O. Gunnarsson, K. Schönhammer, D. Das Sarma, F. U. Hillebrecht, and M. Campagna, Phys. Rev. B **32**, 5499 (1985), and references cited therein.
[36]For a general discussion of inelastic electron scattering we refer to (a) T.-Y. Wu and T. Ohmura, *Quantum Theory of Scattering* (Prentice-Hall, Englewood Cliffs, 1962) and (b) J. Kessler, *Polarized Electrons,* 2nd ed. (Springer-Verlag, Berlin, 1985); for discussions directly related to the present work, see, e.g., Refs. 37–40, in particular Ref. 38.
[37]Y. Itikawa and K. Sakimoto, Phys. Rev. A **31**, 1319 (1985).
[38]S. M. Younger, Phys. Rev. Lett. **56**, 2618 (1986).
[39]M. Pindzola, D. C. Griffin, and C. Bottcher, Phys. Rev. A **34**, 3668 (1986).
[40]M. Ya. Amusia and S. A. Sheinerman, J. Phys. B **12**, 649 (1979).
[41]Calculating the incident and inelastically scattered waves in the same (initial-state) potential $V(r)$ avoids inconsistencies in the perturbation approach. Physically, the inelastically scattered electron sees the $(\underline{d}f)$ final-state potential; the difference potential is fairly short ranged and may be incorporated into an effective $d \rightarrow f$ scattering matrix element via perturbation theory.
[42]Integration over the whole energy range may be justified as well, but then the normalization of the EELS spectrum must account for this.
[43]S. M. Younger, Phys. Rev. A **22**, 111 (1980).
[44]On the other hand, based on qualitative arguments, Netzer, Strasser, and Matthew (Ref. 4) assigned the 101.7-eV peak to $^1H_5$ with only a small amount of $^3D_1$ character. The directly excited $^1H_5$ cross section should be smaller, but not very much smaller, than the $^1F_3$ cross section due to smaller angular and radial transition matrix elements. If one assumes in Fig. 1 that the $^3D_1$ XAS peak should appear with the same intensity relative to ^1P in the 2920-eV EELS, then maybe 50% of the 101.7-eV peak could be due to $^1H_5$. The correct picture might be somewhere in between.
[45]Just considering the calculated multiplicity ($J=1,3,5$) of the 101.7-eV peak (degeneracy $3+7+11=21$) gives a (101.7-eV peak) to ^1F ratio of $\frac{21}{7}=3$. This number also happens to agree with the lowest-energy experimental point in Fig. 13.
[46]Note that the inverse of this ratio was used in Sec. IV B.
[47]R. J. Celotta and D. T. Pierce, Science **234**, 333 (1986).
[48]B. Sinkovic, D. J. Friedman, and C. S. Fadley, J. Magn. Magn. Mater. (to be published).
[49]B. Sinkovic, B. Hermsmeier, J. Osterwalder, D. J. Friedman, and C. S. Fadley, Phys. Rev. Lett. **62**, 478 (1989).
[50]B. Hermsmeier, J. Osterwalder, D. J. Friedman, and C. S. Fadley, Phys. Rev. Lett. **62**, 478 (1989).
[51]C. Carbone, R. Rochow, L. Braichovich, R. Jungblut, T. Kachel, D. Tillmann, and E. Kisker, Phys. Rev. B **41**, 3866 (1990).
[52]R. Rochow, C. Carbone, Th. Dodt, F. P. Johnen, and E. Kisker, Phys. Rev. B **41**, 3426 (1990).
[53]D. P. Pappas, K.-P. Kämper, and H. Hopster, Phys. Rev. Lett. **64**, 3179 (1990).
[54]M. Donath and V. Dose, Europhys. Lett. **9**, 821 (1989).
[55]D. Venus and J. Kirschner, Phys. Rev. B **37**, 2199 (1988).
[56]D. L. Abraham and H. Hopster, Phys. Rev. Lett. **62**, 1157 (1989).
[57]D. Pescia and V. L. Pokrovsky, Phys. Rev. Lett. **65**, 2599 (1990).
[58]D. R. Penn and P. Apell, Phys. Rev. B **38**, 5051 (1988), and references cited therein.